Cenomanian–Turonian oceanic anoxic event (OAE2) imprint on the northwestern part of the Adriatic Carbonate Platform and a coeval intra-platform basin (Istria and Premuda Island, Croatia)

Brčić, Vlatko; Glumac, Bosiljka; Brlek, Mihovil; Fuček, Ladislav; Šparica Miko, Martina

Source / Izvornik: **Cretaceous Research, 2021, 125**

Journal article, Accepted version
Rad u časopisu, Završna verzija rukopisa prihvaćena za objavljivanje (postprint)

https://doi.org/10.1016/j.cretres.2021.104847

Permanent link / Trajna poveznica: https://urn.nsk.hr/urn:nbn:hr:245:872276

Cenomanian–Turonian Oceanic Anoxic Event (OAE2) imprint on the northwestern part of the Adriatic Carbonate Platform and a coeval intra-platform basin (Istria and Premuda Island, Croatia)

Vlatko BRČIĆ[1*], Bosiljka GLUMAC[2], Mihovil BRLEK[1], Ladislav FUČEK[1] and Martina ŠPARICA MIKO[3]

[1]Department of Geology, Croatian Geological Survey, Sachsova 2, 10 000 Zagreb, Croatia

[2]Department of Geosciences, Smith College, Northampton, Massachusetts 01063, USA

[3]Department of Mineral Resources, Croatian Geological Survey, Sachsova 2, 10 000 Zagreb, Croatia

*Corresponding author e-mail: vlatko.brcic@hgi-cgs.hr

Abstract

The Cenomanian–Turonian boundary (CTB) on the intra-Tethyan Adriatic Carbonate Platform (AdCP) is generally characterised by a transition between microbially laminated and/or bioclastic limestones to calcisphere-rich massive limestone with bioturbated intervals, organic-rich interbeds, firmgrounds, as well as neptunian dikes, carbonate turbidites, tempestites and slumped structures. Compilation of the results from two study sites in the northwestern part of the AdCP and from previous research (on Istria Peninsula and islands in the Adriatic Sea in Croatia) provides a more complete overview of geological events and paleoenvironmental conditions that transformed the formerly contiguous shallow-marine environments during this time period. For the first time, a comparison between protected inner-platform area (Barban

section) and a coeval intra-platform basin (Premuda Island section) during the CTB was made. This study utilized a combination of litho-, bio-, and microfacies studies with SEM, EDS, TOC, $\delta^{13}C$ and $\delta^{18}O$ stable isotope analyses. The stratigraphic successions start with shallow-marine carbonate deposits of the Milna Formation that is conformably overlain by the drowned-platform deposits of the Sveti Duh Formation on the platform and by the Veli Rat Formation in the contemporaneously developed intraplatform basin. These deposits are in turn overlain by the Gornji Humac Formation, which represents re-establishment of shallow-marine depositional systems on the AdCP, whereas the deeper water environment persisted in the intra-platform basin until the Santonian.

Despite diagenetic modifications of shallow-marine carbonate deposits, the results of TOC and stable isotope analyses indicate the influence of global Oceanic Anoxic Event 2 (OAE2). Combination of local and regional synsedimentary tectonics and global Late Cretaceous sea-level changes accompanied by anoxic and hypoxic conditions, extinction of numerous benthic foraminifera, diversification and expansion of planktonic foraminifera and calcareous dinoflagellates, provide new insights into the character of the CTB interval in this part of the Tethyan realm.

Keywords: OAE2, Cenomanian–Turonian, Adriatic Carbonate Platform (AdCP), Sv. Duh Formation, Istria, Kvarner.

1. Introduction

This study aims to define the influence of Oceanic Anoxic Event 2 (OAE2, Jenkyns 1980, Scholle et al. 1980; Schlanger et al. 1987; Arthur et al. 1987, 1988, 1990; Tsikos et al. 2004;

Keller et al. 2004; Karakitsios et al. 2010; Pearce et al. 2009; Jarvis et al. 2011, 2015; among others) on two different sites of the generally shallow-marine intra-Tethyan Adriatic Carbonate Platform (AdCP) in present-day Croatia. OAE2 was one of the most severe and globally most extensive paleoenvironmental changes. The event occurred at the Cenomanian–Turonian boundary (CTB; about 93.9 My ago; Jarvis et al. 2011; among others). An extinction event, marine anoxia, burial of large amounts of organic carbon (Schlanger and Jenkyns 1976; Schlanger et al. 1987; Parente et al. 2008), and rise in sea level (Hardenbol et al. 1998; Miller et al. 2005; Voigt et al. 2006; Haq 2014; Sames et al. 2016) clearly define the OAE2. Present-day oceans are well oxygenated thanks to a conveyor-belt circulation and distribution of cold, oxygen-rich waters from high latitudes all the way to the abyssal zone. Approximately half of the oxygen injected into the deep-sea regions is consumed by decomposition of organic matter in the water column. Increasing ocean's nutrient content could stimulate biological productivity leading to widespread anoxia (Meyer and Kump 2008, and references therein). Cenomanian submarine volcanism was interpreted as a trigger for a chain reaction that caused OAE2 (Sinton and Duncan 1997; Kerr 1998; Larson and Erba 1999; Bralower 2008; Keller 2008; Turgeon and Creaser 2008; Du Vivier et al. 2014). One of the consequences of OAE2 was enhanced preservation and deposition of organic matter on a global scale recognized as positive shifts of $\delta^{13}C$ values of carbonate deposits. Peak of the crisis (i.e., disturbed dynamics of the global carbon cycle) lasted between 320 Ky (min.) and 1.04 ± 0.12 My (max.) (Sageman et al. 2006; Strauss 2006; Voigt et al. 2008; Gambacorta et al. 2015; Sullivan et al. 2020). Paleobiological consequences of the crisis included the extinction of approximately 26% of marine animal genera (Raup and Sepkoski 1986; Monnet 2009), and changes in diversity and abundance of planktonic foraminifera and radiolarians (Caron and Homewood 1983; Jarvis et al. 1988; Huber et al. 1999; Culver and Rawson 2004; Erba 2004; Gebhardt et al. 2010), larger foraminifera (Parente et al. 2008; Caus et al. 2009), calcareous nannoplankton (Leckie et al. 2002), as well

as rudists (Philip and Airaud-Crumière 1991; Steuber and Löser 2000). Widespread dysoxic to anoxic paleoenvironmental conditions and biotic crises in the world oceans also left a significant mark on shallow-marine carbonate systems (Jenkyns 1991; Gušić and Jelaska 1993; Hilbrecht et al. 1996; Davey and Jenkyns 1999; Parente et al. 2008; Immenhauser et al. 2008; Elrick et al. 2009; Gertsch et al. 2010; Nagm 2015; Brčić et al. 2017).

This study focuses on shallow-marine carbonate deposits in the wider area of Istria and Kvarner (Barban and Premuda, Croatia, Fig. 1). Starting in early Cenomanian, the stable and uniform shallow-marine AdCP (Fig. 2a) was impacted by synsedimentary tectonism and sea-level changes, resulting in episodes of pelagic influence. Despite sea-level rise, in some parts of the study area synsedimentary tectonism overprinted eustatic changes and created emerged areas surrounding intra-platform basins (Gušić and Jelaska 1990; Vlahović et al. 1994; Tišljar et al. 1998; Korbar et al. 2012; Brčić et al. 2017; Fig. 2b). One of the main contributions of this study is a comparison between protected inner-platform area (Barban section) and a coeval intra-platform basin (Premuda Island section) during the CTB. This comparison was made possible for the first time in the study area by using an integrated litho-, bio-, and chemostratigraphic approach that allowed the recognition of characteristic signatures of the global OAE2 perturbation.

2. Geological Setting of the Study Area

Deposits of the Mesozoic Adriatic Carbonate Platform (AdCP) are currently exposed in an area approximately 800 km long and 200 km wide, from Italy in the northwest, across Croatia, and to Albania in the southeast (Jelaska 2002; Vlahović et al. 2005). These deposits are predominantly shallow-marine carbonate platform successions, typical of the intra-Tethyan

realm (Fig. 2). Their maximum thickness reaches 5000-8000 m with a stratigraphic range from the upper part of lower Jurassic (Toarcian) to the Eocene (AdCP *sensu stricto*). The extensive vertical thickness is the result of synsedimentary tectonics and long-term shallow-marine sedimentation, and was also influenced by subsequent post-Cretaceous formation of thrust-nappe structures. In the study area (Istria and Kvarner, Fig. 1), one of the tectonic phases occurred during the early and late Cenomanian. At the Cenomanian–Turonian boundary, eustatic and synsedimentary tectonics locally established drowned platform environments, but at the same time caused uplift and subaerial exposure of the surrounding areas (Davey and Jenkyns 1999; Velić et al. 2002, 2003; Ćosović et al. 2004; Vlahović et al. 1994, 2002a, 2003, 2005; Korbar et al. 2012; Brčić 2015, 2017; Fig. 2). Eocene ramp-type limestones and synorogenic flysch deposits marked the onset of the Alpine orogenesis in the region (Grandić et al. 1997; Vlahović et al. 2005; Schmid et al. 2008), when the AdCP successions were strongly deformed. The compressional tectonics (Fig. 1b) resulted in the fold-and-thrust structures of the present-day External Dinarides (Tari 2002; Korbar 2009).

Paleogeographically the studied deposits belong to the northwestern part of the AdCP (Fig. 2a). During the Cenomanian the larger (mostly western) part of present-day Istria and Kvarner was subaerially exposed (Vlahović et al. 1994, 2002a, b; Brčić 2015, 2017, Fig. 2b). This study focuses on the eastern areas with deeper-marine deposits where sedimentation continued throughout the Turonian (Barban section; Fig. 2b) and until Coniacian–Santonian (Premuda section; Fig. 2c). The term “deeper-marine” is used for paleoenvironments of intraplatform basins with limited pelagic influence and water depth of less than approximately 150 m. Stratigraphic successions in both localities begin with shallow-marine, middle to upper Cenomanian skeletal mudstone-wackestone-packstone and rudist floatstone (the Milna Formation), followed by Cenomanian–Turonian deeper-marine calcisphere limestones (the Sv. Duh and Veli Rat Formations). The Barban succession ends with Turonian to Coniacian

shallow-marine skeletal and peloidal mudstone-wackestone, alternating with rudist floatstone (the Gornji Humac Formation; Gušić and Jelaska 1990), while the prolonged deeper-marine sedimentation at Premuda Island resulted in the Veli Rat Formation (Fuček et al. 1991).

3. Materials and Methods

The Barban section, named after a nearby settlement of Barban, is located in the south-eastern part of peninsula Istria in Croatia (Figs. 1 and 2). This section was sampled in road cuts from Barban to the Raša river valley and in the quarry on the eastern side of the valley (Fig. 1e). The Premuda section is located on Premuda Island in the south-eastern part of Kvarner Bay. The exposures at Cape Lopata on the south-eastern tip of Premuda were examined and sampled in detail (Fig. 1d and 1f).

3.1. Fieldwork and thin-section microscopy

In the study area, the best quality exposures of continuous limestone successions were sampled (Fig. 1e and 1f). The surrounding area was mapped at a scale of 1:12.500 and 1:25.000. Two detailed stratigraphic sections were measured with a total thickness of 315 m: 175 m of the Barban section and 140 m at Premuda (Fig. 3). Selected lithotypes were sampled and a total of 237 polished slabs and 293 thin sections were made for petrographic and micropaleontological analyses in order to define lithotypes and microfossil assemblages, interpret depositional environments, document diagenetic modifications and select the most suitable samples for geochemical analyses. Biostratigraphic analyses focused on numerous species of benthic and planktonic foraminifera (Fig. 3; Croatian Geological Survey repository of the studied material).

3.2. Stable-isotope Analysis ($\delta^{13}C_{carb}$, $\delta^{18}O_{carb}$)

Stable isotope analysis was carried out on 122 samples (81 from Barban and 41 from Premuda; Fig. 4; Table 1). Small amounts of carbonate powder (homogeneous, micritic, and non-weathered material, excluding areas with carbonate cement and skeletal fragments) were collected from polished slabs using a microscope-mounted microdrill. Stable-isotope analyses were performed using a DeltaXL mass spectrometer at the University of Massachusetts, Amherst, USA. After heating for an hour at 400°C to remove any volatile organic components, samples were reacted at 70°C with 100% anhydrous phosphoric acid (H_3PO_4) for 10 min. Standard isobaric and phosphoric acid fractionation corrections were applied to all data. Internal analytical precision, monitored through daily analysis of carbonate standards, was better than or equal to 0.1‰ for both carbon and oxygen isotope values. Results are expressed as $\delta^{13}C$ and $\delta^{18}O$ values in ‰ relative to the Vienna PeeDee Belemnite standard (VPDB).

3.3.TOC and Insoluble Residue Analyses

Total organic carbon (TOC; Fig. 5) was measured on mechanically pulverized limestone samples (i.e., bulk powdered micrite), obtained by drilling micritic limestone with a 1 mm diameter drill-bit. A representative weight (10 g) of each sample was treated with hydrochloric acid (4.2M HCl) for 24 h to eliminate carbonate fractions. To dissolve dolomite that could have been present in the samples the dissolution was performed by heating the hydrochloric acid at 80°C. The samples were filtered and washed several times in distilled water to remove the remaining acid. The insoluble residue (IR) was weighed in tin capsules and analysed using a Thermo Fisher Scientific Flash 2000 NC Elemental Analyser at the Croatian Geological Survey (HGI-CGS). Assuming a complete elimination of carbonate components during the acid treatment, the percentage of IR was calculated using the equation IR = (DM/TM) × 100, where

DM is the weight of the insoluble residue remaining after dissolution of carbonates and TM is the total weight of sample before acid treatment. The amount of TOC_{IR} (%) within IR was determined with elemental analyser and the calculated TOC_{sample} (%) for the whole sample was calculated as TOC_{sample} (%) = (DM/TM) X TOC_{IR} (%). The calibration accuracy was verified by measuring samples of certified Soil Reference Material NC (Thermo Scientific), treated in the same way as the samples. Standard quality check analysis of internal standards performed at HGI-CGS yielded a relative standard deviation (RSD) on TOC measurements of 0.4%.

4. Results

The Barban section is composed of three lithostratigraphic units: the Milna (38 m in thickness), Sv. Duh (116 m) and Gornji Humac Formations (21 m; Gušić and Jelaska 1990; Figs. 3 and 4). The Premuda section contains two lithostratigraphic units: the Milna (30 m thick; Gušić and Jelaska 1990) and Veli Rat Formations (110 m; equivalent of the Sv. Duh Formation with prolonged deeper-marine sedimentation; Fuček et al. 1991; Figs. 3 and 4).

Well-stratified, shallow-marine, middle to upper Cenomanian, foraminiferal wackestone–packstone, alternating with bioclastic (rudist and chondrodontid bivalves) floatstone and microbial laminites, represent the Milna Formation (Figs. 3, 6, 7 and 8). These deposits underlie a drowned-platform succession of the Sv. Duh Formation. Transition between the Milna and Sv. Duh (or its equivalent Veli Rat) Formations can be gradual (laminites and/or bioclastic limestone replaced with progressively thicker intercalations of calcisphere mudstone-wackestone, e.g. Barban section) or sharp (the well-stratified lithotypes overlain by massive calcisphere-rich limestone, e.g. Ćićarija sections in Brčić et al. 2017). The Sv. Duh Formation consists of 116 m of massive calcisphere wackestone with rare fine-grained bioclastic

intercalations and sporadically enriched in organic matter formed in deeper-marine settings of the temporarily submerged/drowned carbonate platform with a significant open-ocean influence. Typical characteristics of these deposits are greyish to light brown erosional surfaces, poorly stratified to massive mudstone-wackestone with calcareous dinoflagellate cysts, fine-grained carbonate bioclasts, planktonic foraminifera, ostracods, pelagic crinoids, sponge spicules, echinoid spines, rare benthic foraminifera, thin-shelled bivalves, and gastropods. Other characteristics include bioturbation, dissolution seams, current microlamination, and undulated upper bedding planes. Stratigraphic range of this unit is late Cenomanian–early Turonian. Unlike the Sv. Duh Formation, the Veli Rat Formation is characterised by carbonate turbidites reflecting a different setting and prolonged deeper-marine sedimentation (late Cenomanian–early Santonian; for a more detailed explanation see Sections *4.2.* and 5). The uppermost well-stratified shallow-marine succession belongs to the Gornji Humac Formation characterised by fenestral mudstone, bioclastic-peloid-skeletal wackestone and radiolitid floatstone (with rudist debris, benthic foraminifera, echinoid spines, fine carbonate detritus, and peloids). Transition between the Sv. Duh and Gornji Humac Formations is commonly defined by a shallowing-upward trend (in some cases by oncoid and laminites facies). Deposits in the lower part of Gornji Humac contain shallow-marine bioclastic material mainly composed of rudist debris, benthic foraminifera, crinoids, echinoid spines, fine carbonate detritus, and peloids that infilled intraplatform depressions. Stratigraphic range of the Gornji Humac Formation is middle Turonian-Coniacian (Figs. 3, 6, 7 and 8; for a more detailed explanation see Sections *4.1.* and 5).

4.1. The Barban section

The Barban section (Figs. 3 and 4) starts with shallow-marine peloid-skeletal-bioclastic wackestone–packstone alternating with microbial laminites and sporadic rudist bioclastic

floatstone. Dominant allochems are benthic foraminifera, rudist debris, fine-grained carbonate bioclasts and detritus, ostracods, fragments of dasycladal algae and rare *Decastronema kotori* (Radoičić) and *Thaumatoporella parvovesiculifera* (Raineri). The presence of benthic foraminifera *Pastrickella balcanica* (Cherchi, Radoičić and Schroeder) *Chrysalidina gradata* d'Orbigny, and *Vidalina radoicicae* Cherchi and Schroeder stratigraphically defines these deposits as middle to upper Cenomanian and as the uppermost part of the Milna Formation (Fig. 9).

Transition between the Milna and Sv. Duh Formations (42 m from the bottom of Barban section, Fig. 7b) begins with successive intercalations of deeper-marine fine-grained bioclastic calcisphere wackestone within predominantly shallow-marine bioclastic to skeletal packstone. Above these 2 m thick transitional deposits, the bioclastic lithofacies is replaced by thick-bedded to massive calcisphere mudstone to wackestone with planktonic foraminifera (*Rotalipora* sp., *Praeglobotruncana* sp. and *Heterohelix* sp.), ostracods, pelagic crinoids, sponge spicules, echinoid spines, bivalve bioclasts, and fine carbonate detritus. Exposures of this interval are characterised by greyish-light to brown colour, and by their brittle, fractured, partly recrystallized, and thick-bedded to massive appearance. Stratigraphically these 98 m thick deposits belong to the uppermost Cenomanian to middle Turonian and represent the deeper-marine Sv. Duh Formation (Fig. 10).

An 18 m thick interval (between 136 and 154 m of the Barban section) is characterised by a shallowing-upward trend represented by cross-bedded and fining upward grainstone followed by calcisphere wackestone. The sharp contact (at 136 m) between the grainstone and wackestone is marked by prominent stylolites (Figs. 3, 4 and 7d). This part of the section represents a transition between the Sv. Duh and Gornji Humac Formation.

The uppermost 21 m of the succession consists of shallow-marine bioclastic floatstone of the Gornji Humac Formation with radiolitid rudists *Distefanella* sp. and thin-shelled bivalves

(*Exogyra* sp.), alternating with fenestral mudstone and bioclastic-peloid-skeletal wackestone. The stratigraphic range of the Gornji Humac Formation in the wider study area is middle Turonian to Coniacian, based on the presence of *Distefanella* sp. and *Hippurites requieni* Matheron, *Decastronema kotori* (Radoičić), *Thaumatoporella parvovesiculifera*, *Moncharmontia* sp., *Pseudocyclammina sphaeroidea* Gendrot, *Scandonea samnitica* De Castro, *S. mediterranea* (De Castro), *Dicyclina schlumbergeri* Munier-Chalmas and *Murgella lata* Luperto-Sinni (Velić 2007; Figs. 3 and 4).

4.2. The Premuda section

The Premuda section (Figs. 3 and 4) starts with the Milna Formation shallow-marine peloidal-skeletal wackestone–packstone, sporadically alternating with slightly undulating microbial laminites, peloidal packstone–grainstone and rudist lithostromes (Fig. 8a). The most common skeletal allochems are benthic miliolid and nezzazatid foraminifera. Index benthic foraminifera *Pastrickella balcanica* (Cherchi, Radoičić and Schroeder), *Chrysalidina gradata* d'Orbigny, *Vidalina radoicicae* Cherchi and Schroeder, *Pseudorhapydionina dubia* De Castro (Fig. 9) clearly indicate middle to late Cenomanian age for the top of Milna Formation. Rudist debris and in places whole radiolitid shells make up the lithostrome interlayers. The remaining allochems include fine-grained carbonate bioclasts and detritus, ostracods, echinoid spines, crinoids, and fragments of dasycladal algae (*Heteroporella lepina* Praturlon). This interval also features bioturbated interlayers, a neptunian dike (at 13 m of the section) and undulated upper bedding planes.

Relative to other localities and sections in the surrounding area, the transition between Milna and Veli Rat Formations at Premuda is atypical. At 30 m of the section (Figs. 3 and 4), there is a first 2.5 m thick layer of calcisphere wackestone–packstone with increased proportion of fine bioclasts, overlain by 4 m of shallow-marine lithotypes. This pattern is repeated for the next 24

m. The proportion of fine bioclasts in the calcisphere wackestone–packstone decreases upwards and the thickness of the deeper-marine deposits increases. The shallow-marine unit becomes more thinly bedded and with a higher proportion of radiolitid bioclasts upsection. Deeper-marine limestones dominate the stratigraphic interval between 44 and 140 m. Within this interval, from 44 to 60 m, there are two up to a meter-thick lenticular intercalations of coarse-grained bioclastic-lithoclastic floatstone (Figs. 8b, 8c, 8d and 8e). Farther upsection, from 60 to 102 m, the intercalations are thinner and characterised by fine-grained bioclastic packstone (up to 0.5 m thick lenses at every 5 to 10 m of the section). From 102 m to the top of the section there are no intercalations of platform-derived bioclastic limestone and the succession contains only pelagic allochems.

Based on the first appearance of thick-bedded to massive calcisphere wackestone–packstone, the 30–140 m interval of Premuda section is attributed to the Veli Rat Formation. This interval contains calcareous dinoflagellates, planktonic foraminifera, ostracods, pelagic crinoids, sponge spicules, echinoid spines, fine bivalve bioclasts, and undefined carbonate detritus. Identified planktonic foraminifera include: *Whiteinella archaeocretacea* Pessagno, *Helvetoglobotruncana praehelvetica* (Trujillo), *Whiteinella* cf. *paradubia* (Sigal), *Dicarinella primitiva* (Dalbiez), *Dicarinella imbricata* (Monrod), *Praeglobotruncana* cf. *algeriana* (Caron), *Rotalipora* sp., *Praeglobotruncana* sp., *Praeglobotruncana gibba* (Klaus), *Helvetoglobotruncana* cf. *helvetica* (Bolli), *Marginotruncana sigali* (Reichel), *Archaeoglobigerina* cf. *cretacea* (d'Orbigny), *Archaeoglobigerina* cf. *blowi* Pessagno, and *Heterohelix* sp. (Fig. 10). Index planktonic foraminifera indicate the lower Turonian to lower Coniacian stratigraphic range (Caron 1985).

4.3. Stable-isotope Data ($\delta^{13}C_{carb}$, $\delta^{18}O_{carb}$) of Bulk Micrite

Sampling of the stratigraphic sections for carbon and oxygen isotope analysis targeted the CTB interval with the intention of comparing the results with the European carbon-isotope reference curve from Eastbourne (Gun Gardens, England; Paul et al. 1999; Jarvis et al. 2006; Pearce et al. 2009; Figs. 4 and 5). Micritic carbonate components were sampled from the 20 to 135 m section interval at Barban, and from 18 to 97 m at Premuda. The Barban section samples have $\delta^{13}C$ values ranging between 0.71 and 3.77‰ and $\delta^{18}O$ between -5.64 and -0.98‰, and the Premuda samples yielded $\delta^{13}C$ values of -0.96 to +4.13‰ and $\delta^{18}O$ values of -6.58 to -3.48‰ (Fig. 5; Table 1). The Barban section shows a certain degree of covariance between the $\delta^{13}C$ and $\delta^{18}O$ data (for a more detailed explanation see Section 5). The Premuda section has no significant covariance between the $\delta^{13}C$ and $\delta^{18}O$ data (Fig. 5).

4.4. Carbon isotope values ($\delta^{13}C_{carb}$) of the Barban section

The first sample for stable isotope analysis was collected in the Milna Formation at 20.5 m of the Barban section. The $\delta^{13}C$ values start at about 3.0 ‰ and for the next 10 m they gradually decrease to 2.5 ‰ (Fig. 4). The 30-45 m interval (the uppermost Milna Formation) is characterised by fluctuations in $\delta^{13}C$ values between 2.0 and 4.0 ‰. At 45 m of the Barban section, in the Sv. Duh Formation, there is a steep decrease in $\delta^{13}C$ values from 3.0 to 0.75 ‰. In the overlying 10 m (45-55 m of the section) the values vary between 0.75 and 2.1‰. At 56 m of the section, the values sharply increase to 3.5 ‰. In the following 24 m (56-80 m) the values remain relatively uniform (around 3.0 ‰) and without major oscillations. At 80 m of the section there is another positive shift in $\delta^{13}C$ values from 3.0 ‰ to 4.0 ‰. The values remain relatively high (between 3.5 and 4.0 ‰) in the next 25 m (105 m of the section). The interval from 105 to 115 m of the section revealed a decline from 4.0 to 2.4 ‰ in $\delta^{13}C$ values. In the following 2 m the values increase to 3.5 ‰ (at 117 m of the section) and for the rest of the succession (117-135 m) they vary between 3.0 and 3.5 ‰ (Figs. 4 and 5; Table 1).

4.5. Oxygen isotope values ($\delta^{18}O_{carb}$) of the Barban section

Starting with -0.1 ‰ at 20.5 m in the Milna Formation of the Barban section, the $\delta^{18}O$ values decrease gradually to -3.9 ‰ for the next 13 m (Fig. 4). The interval from 33 m to 45 m of the section is characterised by significant fluctuations in $\delta^{18}O$ values between -2.7 and -5.4 ‰, with a generally decreasing-upward trend. For the next 10 m (45–55 m of the section) the $\delta^{18}O$ curve oscillates between -5.4 and -4.3 ‰. Above this interval, a general shift towards positive values is maintained for 30 m of the section. Between 55 and 85 m, the values increase upsection and vary from -5.5 to -3.2 ‰. For the rest of the section the values vary slightly between -3.9 and -3.0 ‰ (Figs. 4 and 5; Table 1).

4.6. Carbon isotope values ($\delta^{13}C_{carb}$) of the Premuda section

The first sample collected in the Milna Formation at 18 m of the Premuda section has a $\delta^{13}C$ value of -0.5 ‰ (Fig. 4). For the next 2 m the $\delta^{13}C$ values increase to 2.2 ‰ followed by a sharp decline to -0.7 ‰ (at 25 m of the section). The next 5 m record an increase to the highest $\delta^{13}C$ value of 4.0 ‰ at the transition between Milna and Veli Rat Formations. The 30-42 m interval is characterised by fluctuating, but generally decreasing values, reaching the minimum of -1.0 ‰. An upward shift to positive values (up to 4.0 ‰ at 55 m of the section) in the 42-59 m interval is also marked by pronounced fluctuations. For the next 12 m (60–72 m) the carbon-isotope curve follows a decreasing trend from 4.0 to 0.5 ‰. A recovery to a maximum value of 4.1 ‰ occurs at 74 m of the Premuda section, and the uppermost 23 m (74-97 m) show the values decline to 2.8 ‰ in an oscillating fashion (Figs. 4 and 5; Table 1).

4.7. Oxygen isotope values ($\delta^{18}O_{carb}$) of the Premuda section

The Premuda section samples show a considerable variation in their $\delta^{18}O$ values from -6.6 to -3.5 ‰. Initially the values show a slight increase from -4.5 ‰ at 18 m of the section to -3.5 ‰ at 30 m, followed by a sharp decline to -6.6 ‰ at 34 m at the transition between Milna and Veli Rat Formations (Fig. 4). In the next 18 m (30-48 m) the values fluctuate between -6.6 and -4.6 ‰. The fluctuating trend continues upward to the top of the section (48–97 m), with a change in the slope of the curve towards slightly more positive values. The lowest values (-6.0 to -5.5 ‰) are recorded at 55, 74, 84 and 92 m, and the highest values of -4.5 to -4.3 ‰ come from 68, 80 and 86 m (Figs. 4 and 5; Table 1).

4.8. TOC and Insoluble Residue Analysis

The variations in TOC and insoluble residue from the Barban section are shown in Figure 5 and Table 1. To display the relationship of TOC/insoluble residue/stable-isotope data of relatively pure carbonates (shallow-marine limestones) the TOC values are multiplied by 100 (Fig. 5). In the lowermost 23 m of the Barban section (20-43 m) the TOC values oscillate between 0.02 and 0.7 ‰. In the next 2 m (43–45 m) the TOC reaches the highest value of 1.8 ‰ at the transition between Milna and Sv. Duh Formations, followed by a sharp decline (45–47 m) to 0.2 ‰. For the next 48 m (47–95 m) the TOC curve shows fluctuations with a generally increasing upward trend from 0.2 to 0.8 ‰. For the rest of the section the TOC values show somewhat less variation and a general upward decrease from 0.8 to 0.1 ‰. The insoluble residue curve (clay minerals and quartz) coincides with the TOC one, from a minimum value of -0.13 % and the maximum of 2.47 %. Noticeable fluctuations in the insoluble residue values were observed at intervals 37–46 m, 83–96 m and 114–121 m (Fig. 5).

5. Interpretations and Discussion

Despite local and regional mid-Cretaceous synsedimentary tectonism and late Cenomanian global sea-level changes, the paleoenvironmental conditions throughout the AdCP remained relatively stable and highly productive throughout this time (Gušić and Jelaska 1990; Vlahović et al. 2005; Tišljar et al. 1998; Cvetko Tešović et al. 2011; Korbar et al. 2012; Brčić et al. 2017; Picotti et al. 2019). Post-Cenomanian tectonic changes, however, served as a prelude for a transition in depositional geomorphology from rimmed carbonate platform (Paleocene) to a ramp (Eocene). In the study area during the CTB interval, synsedimentary tectonism locally overprinted eustatic changes and laterally created uplifted areas undergoing subaerial exposure coeval with the existence of intra-platform basins (Brčić et al. 2017; Fig. 6). This caused a pronounced lateral differentiation of the AdCP facies (Tišljar et al. 1994, 1998, 2002; Vlahović et al. 1994, 2002a, b, 2005; 2011; Velić et al. 2002, 2003). The processes of karstification and the formation of paleorelief affected the emerged parts of western AdCP (upper part of the Milna Formation). Tectonically and eustatically drowned areas (i.e., intra-platform basins) experienced deeper-marine depositional conditions (see Fig. 6) as reflected in the transition into the overlying Sv. Duh and Veli Rat Formations.

5.1. Shallow-marine facies

The upper parts of the Milna Formation are characterised by intensive carbonate bioproduction (dominant contribution of biomaterial in the form of large benthic foraminifera and rudist bioclasts; Fig. 4 and Fig. 9). Cenomanian foraminiferal assemblages in the study area are probably the richest in the entire succession of shallow-marine carbonates (from the Toarcian to the Santonian; Velić 2007). Cyanobacterial laminites predominate in the top few meters of the Milna Formation, and sporadic fenestral mudstones with laminites indicate the minimum

399 water levels in large parts of the carbonate platform (Raspini 2012). The upper part of the Milna
400 Formation is represented by the shallow-marine carbonate platform facies in the first 42 m of
401 the Barban section and 30 m of the Premuda section (Fig. 4; Gušić and Jelaska 1990). Peloid-
402 skeletal wackestone–packstone alternating with microbial laminites and sporadic rudist
403 bioclastic floatstone with fine-grained carbonate bioclasts, ostracods, fragments of dasycladal
404 algae and crinoids were formed in protected environments, ranging from shallow subtidal,
405 across intertidal to tidal flats (Fig. 6a). Detailed descriptions of this paleoenvironment are
406 provided by Korbar et al. (2001), Steuber et al. (2005), and Korbar and Husinec (2003; Kvarner
407 area; Fig. 1).
408 Late Cenomanian in the study area is characterised by the presence of benthic foraminifera
409 *Pastrickella balcanica* (Cherchi, Radoičić and Schroeder), *Vidalina radoicicae* Cherchi and
410 Schroeder, *Chrysalidina gradata* d'Orbigny, and *Pseudorhapydionina dubia* De Castro (Fig.
411 9). In addition, there are also *Cisalveolina* sp., *Peneroplis planatus* (Fichtel & Moll), *Scandonea*
412 sp., *Cuneolina* cf. *pavonia* (d'Orbigny) *Pseudonummoloculina heimi* (Bonet), *Idalina* cf.
413 *antiqua* (Munier-Chalmas et Schlumberger), *Nezzazata* cf. *gyra* (Smout), and *Nezzazata*
414 *simplex* (Omara). Following the biozonations of Velić (2007), Chiocchini (2008) and Frijia et
415 al. (2015), this interval belongs to the *Chrysalidina gradata* benthic foraminifera biozone.
416 At the Barban section, following the carbonate platform drowning at the CTB, a minor
417 regressive phase and infilling of intraplatform basins with shallow-marine paleoenvironmental
418 conditions were re-established in middle Turonian (Fig. 6c). The stratigraphic interval from 154
419 to 175 m in the Barban section belongs to the Gornji Humac Formation. Its middle Turonian to
420 Coniacian age is defined by the presence of *Distefanella* (Henhöfer et al. 2014) and *Hippurites*
421 *requieni* Matheron rudists, *Moncharmontia* sp., *Pseudocyclammina sphaeroidea* Gendrot,
422 *Scandonea samnitica* De Castro, S. *mediterranea* (De Castro), *Dicyclina schlumbergeri*
423 Munier-Chalmas and *Murgella lata* Luperto-Sinni benthic foraminifera, but also *Decastronema*

kotori (Radoičić) and *Thaumatoporella parvovesiculifera*. Coniacian limestones of the Gornji Humac Formation at the Barban section represent the last deposits of the AdCP in this area. Unlike the above, the Veli Rat Formation at the Premuda section continued with deeper-marine sedimentation into the Santonian (see Section *5.3.* Figs. 3 and 6).

5.2. Transition from shallow-marine to deeper-marine facies

In contrast with the Cenomanian, the Turonian on AdCP (and surrounding shallow-marine carbonate platforms) is characterised by a decrease in the diversity and abundance of benthic foraminiferal assemblages as a consequence of global sea-level rise in the latest Cenomanian and earliest Turonian (Gušić and Jelaska 1990; Velić 2007; Parente et al. 2008). Transition between the Milna and Sv. Duh Formations at the Barban section is a typical example of oscillatory transgression (series of cyclic steps generally showing a deepening upward trend). The stratigraphic interval between 40 and 44 m contains several successive repetitions of shallow-marine bioclastic material and micritic intercalations with pelagic influence. The same transition in the Premuda section has characteristic features of the proximal part of the carbonate turbidite facies with reworked, poorly sorted bioclastic breccias found inside the deeper-marine calcisphere mudstone-wackestone (Colacicchi and Baldanza 1986; Fuček et al. 1991; Moro and Ćosović 2013). These changes are repeated throughout the 30–54 m interval of the Premuda section. Occasionally there are slope-derived slump structures associated with fine-grained, reworked benthic platform bioclasts and autochthonous pelagic material with the appearance of neptunian dykes. These deposits indicate that Premuda, unlike the Barban section, was located on the intraplatform basin margins during the CTB (Figs. 2a and 6). Benthic fossils in bioclastic input within the transitional zone are represented with index foraminifera *Pastrickella balcanica* (Cherchi, Radoičić and Schroeder), *Vidalina radoicicae* Cherchi and Schroeder,

449 *Chrysalidina gradata* d'Orbigny, *Cisalveolina* sp., and *Pseudorhapydionina dubia* De Castro.
450 The CTB is also characterised by resedimented upper Cenomanian index benthic foraminifera
451 within autochthonous pelagic layers of the transitional zone with planktonic foraminifera
452 (*Whiteinella archaeocretacea*, *W. praehelvetica*, *W.* cf. *paradubia*, *Rotalipora* sp. and
453 *Praeglobotruncana* sp.).
454
455 *5.3. Deeper-marine facies*
456 The total thickness of the Sv. Duh Formation deposits in the Barban section is 116 m.
457 Stratigraphically these deposits are entirely Turonian, and have a sharp transition into the
458 overlying shallow-marine Gornji Humac Formation (Turonian–Coniacian). Unlike Barban, the
459 Premuda section reveals a prolonged deeper-marine sedimentation (the Veli Rat Formation).
460 The youngest pelagic fossils from the upper part of the Premuda section are of Coniacian age
461 (*Marginotruncana sigali*, *Dicarinella* sp., *Archaeoglobigerina* cf. *cretacea*, *A. blowi*; Fig. 10).
462 Geological mapping of the wider area of the island also revealed some even younger pelagic
463 deposits (Santonian; Moro and Ćosović 2013; Fuček et al. 2018). The difference in
464 paleogeographic location of the individual sections is also evident in the dominance of pelagic
465 components at Premuda (dinoflagellate cysts and planktonic foraminifera; Figs. 4 and 6). The
466 pelagic deposits are about 100 m thick in both stratigraphic sections. At Barban the complete
467 pelagic interval formed during the latest Cenomanian and almost the entire Turonian (in the
468 span of approximately 5 million years, Cohen et al. 2018). At the Premuda section, the same
469 interval was deposited from the latest Cenomanian through the beginning of Coniacian
470 (approximately 6 million-year span, Cohen et al. 2018). The main reason for lower depositional
471 rates and/or smaller thickness of the Premuda deposits (i.e., the Veli Rat Formation) is the
472 difference in their paleoenvironment. The Premuda section was situated on the margin of an
473 intraplatform basin, which resulted in greater accommodation space and stronger open ocean

474 influence, but was characterised by lower depositional rates (see Fig. 3 for the relationship
475 between thickness and stratigraphic intervals). In contrast, the Barban section was likely located
476 in a more protected intraplatform area where high bioclastic production (see Figs. 2 and 6) and
477 small accommodation space resulted in faster infilling and shallowing of the drowned platform
478 facies (i.e., the Sv. Duh Formation). Thus, Barban is characterised by a greater thickness of the
479 CTB drowned platform succession (constant backfill of fine bioclastic material from the
480 surrounding areas resulted in thicker pelagic successions).
481 Early–middle Turonian global eustatic sea-level fall (Hardenbol et al. 1998; Miller et al. 2005;
482 Voigt et al. 2006; Haq 2014; Sames et al. 2016) caused a faster backfill of intraplatform
483 depressions with bioclastic material (mainly fragments of rudist colonies and benthic
484 foraminifera) from the surrounding shallow-marine areas (Gušić and Jelaska 1993; Korbar et
485 al. 2001). This process is clearly visible in the Barban section at the 136–175 m interval
486 (transition between the Sv. Duh and Gornji Humac Formations). The re-establishment of
487 shallow marine depositional environments in the late Turonian was characterised by gradual
488 recolonization of rudists and benthic foraminifera, but with lower richness of taxa and smaller
489 number of specimens relative to the Cenomanian (Velić 2007). At the Premuda section, the
490 shallow-marine deposits of the Gornji Humac Formation (the upper boundary of the Veli rat
491 Formation) are buried under the recent Adriatic Sea deposits (Fig. 1f) and are thus inaccessible
492 for direct observation.
493
494
495 *5.4. Stable isotope, TOC and insoluble residue data*
496 Chronostratigraphic calibration of Upper Cretaceous shallow-marine carbonate platform
497 deposits of the Tethyan area is commonly hindered by low-resolution stratigraphic schemes due
498 the lack of chronostratigraphic markers such as ammonites, planktonic foraminifera and

calcareous nannoplankton (Fleury 1980; De Castro 1991; Chiocchini et al. 2008; Velić 2007). For this reason, isotope geochemistry ($\delta^{13}C$ and $\delta^{18}O$) is currently the best available stratigraphic tool (Frijia et al. 2015; Brčić et al. 2017). The results of stable isotope analysis (Table 1; Fig. 5) were used to improve stratigraphic interpretations and global correlation of the studied deposits. The challenging aspects of this part of the research were the limited number of samples, tectonically disturbed successions, and diagenetic modifications. Recrystallization of carbonate mud is the main diagenetic process that impacted the carefully selected micritic samples without obvious carbonate cement and skeletal fragments. Nevertheless, the study produced isotope curves that show significant correlation with the informal reference curves of basinal successions (Paul et al. 1999; Jarvis et al. 2006; Pearce et al. 2009; Fig. 5). During the Cenomanian and Turonian there was no terrigenous input to the north-western part of the isolated AdCP (Fig. 2a). Even though the interiors of large carbonate platform are commonly isolated and subject to localized environmental fluctuations, global events such as OAE2 (Jenkyns 1980, 2010; Schlanger et al. 1987; Arthur et al. 1987, 1988, 1990; Paul et al. 1999; Tsikos et al. 2004; Keller et al. 2004; Pearce et al. 2009; Jarvis et al. 2011; among others) and sea level maxima (Haq 2014) were large enough in scope to overprint local influences and get recorded and preserved in the depositional succession of the AdCP shallow-marine settings regardless of diagenetic modifications (Jenkyns 1991; Gušić and Jelaska 1993; Hilbrecht et al. 1996; Davey and Jenkyns 1999; Parente et al. 2008; Immenhauser et al. 2008; Elrick et al. 2009; Gertsch et al. 2010; Nagm 2015; Brčić et al. 2017). These influences are evident in the drowned platform facies of the northwestern part of the AdCP (Fig. 6b), oxygen-restricted paleoenvironmental conditions and intervals of carbonate factory crisis reflected in bioturbation (Fig. 3), sulphate reduction, synsedimentary pyrite and greenish glauconite (other sections in Istria, Ćićarija, Brčić et al. 2017). The nearest previously examined OAE2 sedimentary successions are carbonate-free black shales in Italy (Gubbio; Coccioni and Luciani 2005),

524 Austria (Rehkogelgraben; Wagreich et al. 2008) and Greece (Ionian zone; Karakitsios et al.
525 2007, 2010). However, the results of carbon and oxygen isotope analyses were here compared
526 to chalk deposits from Eastbourne Gun Gardens (Fig. 5) because they currently represent the
527 best reference curve for this stratigraphic interval. This reference curve records the pre-
528 excursion levels, the first build up (or peak *a*), the trough, the second build-up (peak *b*), and the
529 plateau (ending with peak *c*; Paul et al. 1999; Tsikos et al. 2004).
530 Facies variation and diagenesis may limit the reliability of $\delta^{13}C$ data from the same interval
531 within a single section (Immenhauser et al. 2008; Wendler 2013; Jarvis et al. 2015). The
532 covariance between $\delta^{13}C$ and $\delta^{18}O$ data (correlation coefficient is 0.74) observed in the Barban
533 section (Fig. 5) suggests that carbon isotope values here may have been affected by diagenetic
534 modifications (such as recrystallization in the presence of meteoric fluids; Swart and Oehlert
535 2018). Despite this diagenetic potential, the similarity with Premuda carbon-isotope record,
536 which shows less covariance with $\delta^{18}O$ values (correlation coefficient is 0.19), and the ability
537 to correlate these local sections with the global reference curve, regardless of major differences
538 in their thickness and lithology (Figs. 3 and 5), supports the application of carbon-isotope
539 stratigraphy in this research regardless of its limitations. Such application was made possible
540 by careful integration of chemostratigraphy with detailed litho- and biostratigraphic data (Figs.
541 3-5 and 7-10), and was also aided by TOC and insoluble residue data.
542 The $\delta^{18}O$ values of diagenetically modified carbonates are mainly controlled by fluid
543 composition, temperature and water/rock ratios (Brand and Veizer 1981). In most Cretaceous
544 carbonates (Scholle and Arthur 1980), the $\delta^{18}O$ data show significant depletion at CTB,
545 suggesting meteoric water influence (Hajikazemi et al. 2010). Similary, the $\delta^{18}O$ values of the
546 Barban section are diagenetically modified, but the $\delta^{18}O$ values of Premuda section generally
547 coincide with the global trend interpreted to reflect the warmest conditions at end of
548 Cenomanian (Jarvis et al. 2011). Despite diagenetic modifications of oxygen-isotope values

549 that limit their potential as paleoenvironmental proxies, the carbon-isotope ratios of the same
550 samples are expected to be more resilient to diagenetic resetting and to more closely resemble
551 the original depositional signatures (Marshall 1992; Parente et al. 2007). Departures towards
552 more negative $\delta^{13}C$ values are interpreted as a consequence of interaction with fluids enriched
553 in ^{12}C derived from organic-matter degradation (Irwin et al. 1977). Compared to Eastbourne
554 $\delta^{13}C$ curve, both research sections show large amplitude in $\delta^{13}C$ variations. The end of peak *a*
555 in both sections is marked by a very abrupt, rapid shift to low $\delta^{13}C$ values, followed by very
556 low values between *a* and *b* peaks. A possible explanation for the observed trends is condensed
557 sedimentation. The rich carbonate production reflected in bioclastic lithotypes of the Milna
558 Formation was abruptly replaced with drowned platform facies (Sv. Duh and Veli Rat
559 Formations) of mudstones with rare dinoflagellate cysts and planktonic foraminifera. These
560 events are closely related to the sharp rise in sea level at the very end of the Cenomanian (Haq
561 2014). Similar examples of condensed sedimentation at CTB can be found locally (Brčić et al.
562 2017), but also in other parts of Tethys realm (Gambacorta et al. 2015; Wohlwend et al. 2015).
563 Furthermore, deposition on carbonate platform shoals and intraplatform basins (depths up to
564 150 m) is highly sensitive to eustatic and tectonic events as reflected, for example, in carbonate
565 turbidite facies of the Veli Rat Formation at Premuda section and bioclastic intercalations of
566 the Sv. Duh Formation at Barban section. This may account for some of the observed
567 fluctuations in $\delta^{13}C$ values (e.g., due to variable rates of organic matter respiration; Patterson
568 and Walter 1994).
569 The results of TOC and insoluble residue analyses (Fig. 5) of shallow-marine deposits from the
570 Barban section indicate low amounts of non-carbonate components (less than 1% on average
571 of clay minerals and quartz), as expected for shallow parts of isolated carbonate platforms. The
572 slightly elevated TOC values at 45 m of the Barban section correlate with the transition from
573 the first build up to the second build-up on the isotope curves (transition Milna–Sv. Duh

574 Formation; Figs. 3 and 5). A similar, but less pronounced change occurred at 81 m of the section
575 and correlates with the transition from the second isotope build-up to the plateau.
576 Stratigraphically, this transition also closely corresponds with the Cenomanian–Turonian
577 boundary and can help determine and position the CTB in the study area (Fig. 5). Correlation
578 coefficient between the TOC and carbon-isotope record at the Barban section is 0.27 (Fig. 5),
579 which suggests that post-depositional alteration in the presence of organic matter played a role
580 in diagenetic history of these deposits (Irwin et al. 1977; Oehlert and Swart 2014). Despite these
581 challenges, the integration of detailed biostratigraphy with TOC/insoluble residue and carbon-
582 isotope records helped determine and position the CTB in the study area, as well as improve
583 stratigraphic resolution through placing stage boundaries and global correlation of Barban and
584 Premuda sections. The first OAE2 geochemical imprint (positive carbon isotope values in
585 response to enhanced organic carbon burial) was detected in uppermost Milna Formation
586 deposits (i.e., the first build up, see Section *5.4* and Fig. 4), preceded by a global rise in sea
587 level at the end of the Cenomanian (Haq 2014). The strongest OAE2 geochemical imprint is
588 recorded in transition from shallow-marine to deeper-marine facies (uppermost Milna
589 Formation deposits to Sv. Duh/Veli rat Formation; peak *b*; see Section *5.4* and Figs. 4 and 5).
590 The OAE2 geochemical imprint within deeper-marine facies interval (Sv. Duh/Veli rat
591 Formation) is represented with the carbon-isotope *c* plateau phase (see Section *5.4* and Figs. 4
592 and 5).
593
594
595 **6. Conclusions**
596
597 1) The Milna, Sv. Duh, Veli Rat and Gornji Humac Formations reflect distinct
598 paleoenvironments that existed at the Cenomanian–Turonian boundary (CTB) in

599 western part of the Adriatic Carbonate Platform (AdCP; Barban and Premuda sections
600 in present-day Croatia). Their deposition was impacted by eustatic sea level changes
601 and synsedimentary tectonics (folding and faulting) resulted in facies differentiation and
602 karstification through uplifts and lowering of individual local platform areas. The
603 Premuda section reveals such tectonic influence (initial forming of intraplatform basins)
604 in combination with sea level rise (pelagic influence).
605 2) The late Cenomanian sea-level rise lead the AdCP into a carbonate factory crisis and
606 condensed sedimentation**.** Bottom and top layers of the intraplatform basin facies of the
607 Veli Rat Formation and the inner platform drowning facies of the Sv. Duh Formation
608 reflect the interplay between the platform drowning and growth (accumulation and
609 aggradation of lateral shallow-marine sediment). Variations in subsidence and
610 accommodation space fine-tuned the depositional processes and stratigraphic record
611 within the research area.
612 3) Global oceanic anoxic event (OAE2) at the CTB left its mark starting from the shallow-
613 marine facies (SMF, Milna Formation), through transitional (TF), and ending in deeper-
614 marine facies (DMF, Sv. Duh and Veli Rat Formations) of the study area. The $\delta^{13}C$
615 values of Barban and Premuda sections indicate that OAE2 impacted the north-western
616 part of AdCP almost entirely in the latest Cenomanian. The observed fluctuations in
617 $\delta^{13}C$ values are evidence of condensed sedimentation and shallow-marine influence.
618 The covariance between $\delta^{13}C$ and $\delta^{18}O$ values at Barban section indicate meteoric
619 diagenesis, but $\delta^{18}O$ values of Premuda section coincide with the global trends
620 interpreted to represent the warmest conditions at the end of Cenomanian. The elevated
621 TOC values at 45 m of the Barban section correlate with the AdCP drowning and a shift
622 to very low $\delta^{13}C$ values. Integration of litho-, bio-, microfacies, and TOC, insoluble
623 residue and stable isotope data indicated a carbonate factory crisis (low sedimentation

rate, drowned platform facies) and geochemical OAE2 imprint at the boundary between the Milna and Sv. Duh/Veli Rat Formations (the latest Cenomanian) in the eastern Istria and southern Kvarner area.

4) Carbon-isotope values from the CTB interval of Barban and Premuda sections in western AdCP represent a combination of global paleoceanographic effects, local environmental factors and diagenetic alteration, and are correlative with the reference curve from English Chalk (Eastbourne, Gun Gardens, England). These correlations contribute towards fine-tuning and calibration of biostratigraphy based on benthic and planktic foraminifera in the study area.

5) Detailed facies interpretations concluded that the Premuda section was located on the margin of an intra-platform basin during the CTB, and the Barban section was in the inner protected areas of the north-western parts of the AdCP. This research contributes an example of integrating the evidence for the influence of global paleoceanographic perturbations on two different (protected platform interior and intra-platform basin) relatively restricted shallow-marine environments with detailed paleogeographic information (emerged, shallow-marine, and drowned platform area) during the CTB in the Tethyan realm.

7. Acknowledgements

This work was supported by the Croatian Geological Survey as part of the project Basic Geological Map of the Republic of Croatia (1:50 000) funded by the Ministry of Science and Education of the Republic of Croatia. We would like to thank Editor-in-Chief Dr. Eduardo Koutsoukos and two anonymous reviewers for useful and comprehensive comments and

suggestions that greatly improved this manuscript. Furthermore, we would like to thank Prof. Stephen Burns (Department of Geosciences, University of Massachusetts, Amherst, USA) for stable isotope analysis and Dr. Lidija Galović (Croatian Geological Survey) for general project support. Dr. Ivan Mišur, Dr. Tomislav Kurečić, Dr. Damir Palenik and MEng. Marko Špelić (Croatian Geological Survey) are thanked for field assistance and help with sampling. Minor contributions towards this research were also made by the GEOTWINN project (Grant no. 809943, EU Horizon 2020).

8. References

Arthur, M.A., Schlanger, S.O., Jenkyns, H.C., 1987. The Cenomanian–Turonian Oceanic Anoxic Event II: palaeoceanographic controls on organic matter production and preservation. In: Brooks, J and Fleet, A (eds.) Marine Petroleum Source Rocks) Geological Society Special Publication 26, 401–420.

Arthur, M.A., Dean, W.E., Pratt, L.M., 1988. Geochemical and climatic effects of increased marine organic carbon burial at the Cenomanian/Turonian boundary. Nature 335, 714–717.

Arthur, M.A., Brumsack, H.J., Jenkyns, H.C., Schlanger, S.O., 1990. Stratigraphy, geochemistry, and paleoceanography of organic carbon–rich Cretaceous sequences. In: Ginsburg, RN, Beaudoin, B (eds.) Cretaceous Resources, Events, and Rhythms. Kluwer Acad. Publ., Netherlands, 75–119.

Blakey, R., 2010. http://jan.ucc.nau.edu/~rcb7/globaltext2.html. Global Paleogeography. NAU Geology, December 2010.

Bralower, T.J., 2008. Earth Science: Volcanic Cause of Catastrophe. Nature, 454, 285–287.

673 Brand, U., Veizer, J., 1981. Chemical diagenesis of a multicomponent carbonate system – 2.
674 Stable isotopes. Journal of Sedimentary Petrology, 51, 987–997.
675 Brčić, V., 2015. Relative sea-level changes during the late Cretaceous in the northwestern part
676 of the Adriatic Carbonate Platform. Doctoral Thesis, University of Zagreb, Faculty of
677 Mining, Geology and Petroleum Engineering, 229.
678 Brčić, V., Glumac, B., Fuček, L., Grizelj, A., Horvat, M., Posilović, H., Mišur, I., 2017. The
679 Cenomanian–Turonian boundary in the northwestern part of the Adriatic Carbonate
680 Platform Ćićarija Mtn., Istria, Croatia): characteristics and implications. Facies 63, 17.
681 Caron, M., Homewood, P., 1983. Evolution of early planktic foraminifers. Marine
682 Micropaleontology 7/6, 453–462.
683 Caron, M., 1985. Cretaceous planktonic foraminifera in Plankton Stratigraphy, H. Bolli, J. B.
684 Saunders, and K. Perch Neilson, Eds., pp. 17–86, University Press, Cambridge, UK.
685 Caus, E., Bernaus, J.M., Calonge, E., Martín-Chivelet, J., 2009. Mid-Cenomanian separation
686 of Atlantic and Tethyan domains in Iberia by a land-bridge: The origin of larger
687 foraminifera provinces? Palaeogeography, Palaeoclimatology, Palaeoecology 283,
688 172–181.
689 Chiocchini, M., Chiocchini, R.A., Didaskalou, P., Potetti, M., 2008. Microbiostratigrafia del
690 Triassico superiore, Giurassico e Cretacico in facies di piattaforma carbonatica del
691 Lazio centro- meridionale e Abruzzo: revisione finale. In: Chiocchini, M. (Ed.),
692 Memorie Descrittive della Carta Geologica d' Italia, Torino, 84, 5–170.
693 Coccioni, R., Luciani, V., 2005. Planktonic foraminifers across the Bonarelli Event (OAE2,
694 latest Cenomanian): The Italian record. Palaeogeography, Palaeoclimatology,
695 Palaeoecology 224, 167–185.
696 Cohen, K.M., Finney, S.C., Gibbard, P.L., Fan, J.-X., 2013 updated. The ICS International
697 Chronostratigraphic Chart. Episodes 36, 199–204.

698 Colacicchi, R., Baldanza, A., 1986. Carbonate turbidites in a Mesozoic pelagic basin: Scaglia
699 formation, Apennines-comparison with siliciclastic depositional models. Sedimentary
700 Geology, 48, 81–105.
701 Culver, S.J., Rawson, P.F., 2004. Biotic Response to Global Change. The Last 145 Million
702 Years. Cambridge University Press, The Natural History Museum, London, 516.
703 Cvetko Tešović, B., Gušić, I., Jelaska, V., Bucković, D., 2001. Stratigraphy and microfacies of
704 the Upper Cretaceous Pučišća Formation, Island of Brač, Croatia. Cretaceous Research
705 22, 591–613.
706 Cvetko Tešović, B., Glumac, B., Bucković, D., 2011. Integrated biostratigraphy and carbon
707 isotope stratigraphy of the Lower Cretaceous (Barremian to Albian) Adriatic-Dinaridic
708 carbonate platform deposits in Istria, Croatia. Cretaceous Research 32, 301–324.
709 Ćosović, V., Drobne, K., Moro, A., 2004. Paleoenvironmental model for Eocene foraminiferal
710 limestones of the Adriatic carbonate platform (Istrian Peninsula). Facies 50, 61–75.
711 Davey, S.D., Jenkyns, H.C., 1999. Carbon-isotope stratigraphy of shallow-water limestones
712 and implications for the timing of Late Cretaceous sea-level rise and anoxic events
713 (Cenomanian–Turonian of the peri-Adriatic carbonate platform, Croatia). Eclogae
714 Geologicae Helvetiae 92, 163–170.
715 De Castro, P., 1991. Mesozoic. In: Barattolo, F., De Castro, P., Parente, M. (Eds.), Field Trip
716 Guide-Book, 5th International Symposium on Fossil Algae. Giannini editore, Napoli,
717 21–38.
718 Du Vivier, A.D.C., Selby, D., Sageman, B.B., Jarvis, I., Gröcke, D.R., Voigt, S., 2014. Marine
719 187Os/188Os isotope stratigraphy reveals the interaction of volcanism and ocean
720 circulation during Oceanic Anoxic Event 2. Earth and Planetary Science Letters 389,
721 23–33.

722 Elrick, M., Molina-Garza, R., Duncan, R., Snow, L., 2009. C-isotope stratigraphy and
723 paleoenvironmental changes across OAE2 (mid-Cretaceous) from shallow-water
724 platform carbonates of southern Mexico. Earth and Planetary Science Letters 277, 295–
725 306.
726 Erba, E., 2004. Calcareous nannofossils and Mesozoic oceanic anoxic events. Marine
727 Micropaleontology 52, 85–106.
728 Fleury, J.J., 1980. L. Publ. Soc. Geol. Du Nord 4 es zones de Gavrovo–Tripolitza et du Pinde–
729 Olnos (Grece continentale et Peloponese du Nord). Evolution d'une plateforme et d'un
730 bassin dans leur cadre alpin, 1–651.
731 Frijia, G., Parente, M., Di Lucia, M., Mutti, M., 2015. Carbon and strontium isotope
732 stratigraphy of the Upper Cretaceous (Cenomanian-Campanian) shallow-water
733 carbonates of southern Italy: Chronostratigraphic calibration of larger foraminifera
734 biostratigraphy. Cretaceous Research, 53, 110–139.
735 Fuček, L., Jelaska, V., Gušić, I., Prtoljan, B., Oštrić, N., 1991. Padinski turonski sedimenti uvale
736 Brbišnica na Dugom otoku. Geološki vjesnik, 44, 55–67.
737 Fuček, L., Korbar, T., Palenik, D., Matičec, D., 2018. Basic Geological Map of the Republic of
738 Croatia scale 1:50.000: sheet Silba 1. Croatian Geological Survey, Department of
739 Geology, Zagreb, ISBN: 978-953-6907-69-4 (in Croatian).
740 Gambacorta G., Jenkyns, H.C., Russo, F., Tsikos, H., Wilson, P.A., Faucher, G., Erba, E., 2015.
741 Carbon- and oxygen-isotope records of mid-Cretaceous Tethyan pelagic sequences
742 from the Umbria-Marche and Belluno Basins (Italy). Newsletters on Stratigraphy, 48,
743 3, 299– 323.
744 Gebhardt, H., Kuhnt, W., Holbourn, A., 2010. Foraminiferal response to sea level change,
745 organic flux and oxygen deficiency in the Cenomanian of the Tarfaya Basin, southern
746 Morocco. Marine Micropaleontology 53/1, 133–157.

747 Gertsch, B., Keller, G., Adatte, T., Berner, Z., Kassab, A.S., Tantawy, A.A.A., El-Sabbagh,
748 A.M., Stueben, D., 2010. Cenomanian–Turonian transition in a shallow water sequence
749 of the Sinai, Egypt. Int. J. Earth Sci. (Geol Rundsch) 99, 165–182.
750 Grandić, S., Boromisa-Balas, E., Šušterčić, M., 1997. Exploration concept and characteristics
751 of the Dinarides in Croatian offshore area. Nafta, 48, 249–267.
752 Gušić, I., Jelaska, V., 1990. Upper Cretaceous stratigraphy of the Island of Brač. Djela
753 Jugoslavenske akademije znanosti i umjetnosti Zagreb 69, 160.
754 Gušić, I., Jelaska, V., 1993. Upper Cenomanian–Lower Turonian sea-level rise and its
755 consequences on the Adriatic-Dinaric carbonate platform. Geol. Rundsch. 82, 676–686.
756 Hajikazemi, E., Al-Aasm, I.S., Coniglio, M., 2010. Subaerial exposure and meteoric diagenesis
757 of the Cenomanian-Turonian Upper Sarvak Formation, southwestern Iran. Geological
758 Society, London, Special Publications, 330, 253–272.
759 Haq, B.U., 2014. Cretaceous eustasy revisited. Global and Planetary Change 113, 44–58.
760 Hardenbol, J., Thierry, J., Farley, M.B., Jacquin, T., Graciansky, P.C., Vail, P., 1998. Mesozoic
761 and Cenozoic sequence chronostratigraphic framework of European Basins, in
762 Graciansky, PC et al. (eds.) Mesozoic and Cenozoic sequence stratigraphy of European
763 basins: SEPM Special Publication 60, 3–13, charts 1–8.
764 Hennhöfer, D.K., Pascual-Cebrian, E., Korbar, T., Stinnesbeck, W., Götz, S., 2014. Radiolitid
765 rudist colonisation strategies and biostrome development in moderate-energy inner-
766 platform environments (Campanian, Brač Island, Croatia). Palaeogeography,
767 Palaeoclimatology, Palaeoecology 403, 80–87.
768 Hilbrecht, H., Frieg, C., Tröger, K.A., Voigt, S., Voigt, T., 1996. Shallow water facies during
769 the Cenomanian-Turonian anoxic event: bio-events, isotopes, and sea level in southern
770 Germany. Cretaceous Research 17/2, 229–253.

771 Huber, B.T., Leckie, R.M., Norris, R.D., Bralower, T.J., Cobabe, E., 1999. Foraminiferal
772 assemblage and stable isotopic change across the Cenomanian–Turonian Boundary in
773 the subtropical North Atlantic. Journal of Foraminiferal Research 29/4, 392–417.
774 Immenhauser, A., Holmden, C., Patterson, W.P., 2008. Interpreting the carbon-isotope record
775 of ancient shallow epeiric seas: Lessons from the Recent. In: Pratt B and Holmden C
776 (eds) Dynamics of epeiric seas. Geological Association of Canada, Special Paper 48,
777 137–174.
778 Irwin, H., Curtis, C., Coleman, M., 1977. Isotopic evidence for source of diagenetic carbonates
779 formed during burial of organic-rich sediments. Nature, 269, 209–213.
780 Jarvis, I., Carson, G.A., Cooper, M.K.E., Hart, M.B., Leary, P.N., Tocher, B.A., Horne, D.,
781 Rosenfeld, A., 1988. Microfossil assemblages and the Cenomanian–Turonian (late
782 Cretaceous) oceanic anoxic event. Cretaceous Research 9, 2–103.
783 Jarvis, I., Gale, A., Jenkyns, H.C., Pearce, M.A., 2006. Secular variation in Late Cretaceous
784 carbon isotopes: a new δ13C carbonate reference curve for the Cenomanian–Campanian
785 (99.6–70.6 Ma). Geological Magazine 143, 561–608.
786 Jarvis, I., Lignum, J.S., Grocke, D.R., Jenkyns, H.C., Pearce, M.A., 2011. Black shale
787 deposition, atmospheric CO2 drawdown, and cooling during the Cenomanian–Turonian
788 Oceanic Anoxic Event. Paleoceanography 26, 2081–2011.
789 Jarvis, I., Trabucho-Alexandre, T., Gröcke, D.R., Uličný, D., Laurin, J., 2015. Intercontinental
790 correlation of organic carbon and carbonate stable isotope records: evidence of climate
791 and sea-level change during the Turonian (Cretaceous). The Depositional Record, 1(2),
792 53–90.
793 Jelaska, V., 2002. Carbonate Platforms of the External Dinarides, in Vlahović, I., Tišljar, J.,
794 eds., Evolution of Depositional Environments from the Palaeozoic to the Quaternary in

795 the Karst Dinarides and Pannonian Basin: 22nd International Association of
796 Sedimentologists, Meeting of Sedimentology, Opatija, Field Trip Guidebook, 67–71.
797 Jenkyns, H.C., 1980. Cretaceous anoxic events: from continents to oceans. Journal of the
798 Geological Society, London 137:171–188.
799 Jenkyns, H.C., 1991. Impact on Cretaceous sea level rise and anoxic events on the Mesozoic
800 carbonate platform of Yugoslavia. The American Association of Petroleum Geologists
801 Bulletin 75/6, 1007–1017.
802 Jenkyns, H.C., 2010. Geochemistry of Oceanic Anoxic Events. Geochemistry Geophysics
803 Geosystems 11/3, 1–30.
804 Karakitsios, V., Tsikos, H., Van Bruegel, Y., Koletti, L., Sinninghe Damsté, S.J., Jenkyns, H.C.,
805 2007. First evidence for the Cenomanian–Turonian oceanic anoxic event (OAE2,
806 “Bonarelli” event) from the Ionian Zone, western continental Greece. International
807 Journal of Earth Sciences (Geol. Rundsch.) 96, 343–352.
808 Karakitsios, V., Kafousia, N., Tsikos, H., 2010. A Review of Oceanic Anoxic Events as
809 recorded in the Mesozoic sedimentary record of mainland Greece. Hellenic Journal of
810 Geosciences 45, 123–132.
811 Keller, G., 2008. Cretaceous climate, volcanism, impacts and biotic effects. Cretaceous
812 Research 29, 754–771.
813 Keller, G., Berner, Z., Adatte, T., Stueben, D., 2004. Cenomanian–Turonian and δ13C, and δ
814 18O, sea level and salinity variations at Pueblo, Colorado. Palaeogeography,
815 Palaeoclimatology, Palaeoecology 211, 19– 43.
816 Kerr, A.C., 1998. Oceanic plateau formation: A cause of mass extinction and black shale
817 deposition around the Cenomanian-Turonian boundary?: Geological Society, London,
818 Journal, 155, 619–626.

819 Korbar, T., 2009. Orogenic evolution of the External Dinarides in the NE Adriatic region: a
820 model constrained by tectonostratigraphy of Upper Cretaceous to Paleogene carbonates.
821 Earth-Science Reviews 96, 296–312.
822 Korbar, T., Husinec, A., 2003. Biostratigraphy of Turonian to (?)Coniacian platform
823 carbonates: a case study from the Island of the Cres (Northern Adriatic, Croatia).
824 Geologia Croatica, 56/2, 173–185.
825 Korbar, T., Fuček, L., Husinec, A., Vlahović, I., Oštrić, N., Matičec, D., Jelaska, V., 2001.
826 Cenomanian carbonate and rudists along shallow intraplatform basin margin – the Island
827 of Cres (Adriatic Sea, Croatia). Facies 45, 39–58.
828 Korbar, T., Glumac, B., Cvetko–Tešović, B., Cadieux, S.B., 2012. Response of a carbonate
829 platform to the Cenomanian–Turonian drowning and OAE 2: A case study from the
830 Adriatic Platform (Dalmatia, Croatia). Journal of Sedimentary Research 82, 163–176.
831 Leckie, R.M., Bralower, T.J., Cashman, R., 2002. Oceanic anoxic events and plankton
832 evolution: biotic response to tectonic forcing during the mid-Cretaceous.
833 Paleoceanography 17, 1041.
834 Larson, R.L., Erba, E., 1999. Onset of the mid-Cretaceous greenhouse in the Barremian–
835 Aptian: Igneous events and the biological, sedimentary, and geochemical responses.
836 Paleoceanography, 14/6, 663–678.
837 Marshall, J.D., 1992. Climatic and oceanographic isotopic signals from the carbonate rock
838 record and their preservation. Geological Magazine 129, 143–160.
839 Miller, K.G., Kominz, M.A., Browning, J.V., Wright, J.D., Mountain, G.S., Katz, M.E.,
840 Sugarman, P.J., Cramer, B.S., Christie-Blick, N., Pekar, S.F., 2005. The Phanerozoic
841 record of global sea-level change. Science 310 (5752):1293–1298.
842 Meyer, K.M., Kump, L.R., 2008. Oceanic euxinia in Earth history: Causes and consequences:
843 Annual Review of Earth and Planetary Sciences, 36, 251–288.

844 Monnet, C., 2009. The Cenomanian–Turonian mass extinction (Late Cretaceous): new insights
845 from ammonoid biodiversity patterns of Europe, Tunesia and Western Interior (North
846 America). Paleogeography Paleoclimatology Paleoecology, 282, 88–104.
847 Moro, A., Ćosović, V., 2013. Upper Turonian–Santonian slope limestones of the Islands of
848 Premuda, Ist and Silba (Adriatic Coast, Croatia). Geologia Croatica, 66/1, 1–13.
849 Nagm, E., 2015. Stratigraphic significance of rapid faunal change across the Cenomanian–
850 Turonian boundary in the Eastern Desert, Egypt. Cretaceous Research 52, 9–24.
851 Oehlert, A.M., Swart, P.K., 2014. Interpreting carbonate and organic carbon isotope covariance
852 in the sedimentary record. Nature Communications, 5, 4672.
853 Parente, M., Frijia, G., Di Lucia, M., 2007. Carbon-isotope stratigraphy of Cenomanian–
854 Turonian platform carbonates from the southern Apennines (Italy): a
855 chemostratigraphic approach to the problem of correlation between shallow-water and
856 deep-water successions. Journal of the Geological Society, London, 164, 609–620.
857 Parente, M., Frijia, G., Di Lucia, M., Jenkyns, H.C., Woodfine, R.G., Baroncini, F., 2008.
858 Stepwise extinction of larger foraminifers at the Cenomanian-Turonian boundary: A
859 shallow-water perspective on nutrient fluctuations during Oceanic Anoxic Event 2
860 (Bonarelli Event). Geology 36/9, 715–718.
861 Patterson, W.P., Walter, L.M., 1994. Depletion of 13C in seawater ΣC02 on modern carbonate
862 platforms: Significance for the carbon isotopic record of carbonates. Geology 22, p.
863 885–888.
864 Paul, C.R.C., Lamolda, M.A., Mitchell, S.F., Vaziri, M.R., Gorostidi, A., Marshall, J.D., 1999.
865 The Cenomanian–Turonian boundary at Eastbourne (Sussex, UK): a proposed European
866 reference section. Palaeogeography, Palaeoclimatology, Palaeoecology, 150, 83–121.
867 Pearce, M.A., Jarvis, I., Tocher, B.A., 2009. The Cenomanian–Turonian event, OAE2 and
868 palaeoenvironmental change in epicontinental seas: New insights from the dinocyst and

geochemical records. Palaeogeography, Palaeoclimatology, Palaeoecology 280, 207–234.

Philip, J.M., Airaud-Crumiere, C., 1991. The demise of the rudist-bearing carbonate platforms at the Cenomanian/Turonian boundary: a global control. Coral Reefs 10, 115–125.

Picotti, V., Cobianchi, M., Luciani, V., Blattmann, F., Schenker, T., Mariani, E., Bernasconi, S.M., Weissert, H., 2019. Change from rimmed to ramp platform forced by regional and global events in the Cretaceous of the Friuli-Adriatic Platform (Southern Alps, Italy). Cretaceous Research 104.

Raspini, A., 2012. Shallow water carbonate platforms (Late Aptian–Early Albian, Southern Apennines) in the context of supraregional to global changes: re-appraisal of palaeoecological events as reflectors of carbonate factory response. Solid Earth, 3, 225–249.

Raup, D.M., Sepkoski, J.J., 1986. Periodic Extinction of Families and Genera. Science, New Series, 231, 4740, 833–836.

Sames, B., Wagreich, M., Wendler, J.E., Haq, B.U., Conrad, C.P., Melinte-Dobrinescu, M.C., Hug, X., Wendler, I., Wolfgring, E., Yilmaz, I.Ö., Zorina, S.O., 2016. Review: Short-term sea-level changes in a greenhouse world – A view from the Cretaceous. Palaeogeography, Palaeoclimatology, Palaeoecology 441, 393–411.

Sageman, B.B., Meyers, S.R., Arthur, M.A., 2006. Orbital time scale and new C–isotope record for Cenomanian–Turonian boundary stratotype. Geology 34/2, 125–128.

Schlanger, S.O., Jenkyns, H.C., 1976. Cretaceous anoxic events: Causes and consequences. Geologie en Mijnbouw 55 (3–4), 179–184.

Schlanger, S.O., Arthur, M.A., Jenkyns, H.C., Scholle, P.A. 1987. The Cenomaniane–Turonian oceanic anoxic event, I. Stratigraphy and distribution of organic-rich beds and the

marine δ13C excursion. In: Brooks, J, Fleet, AJ (eds.) Marine Petroleum Source Rocks. Geological Society, London, Special Publication 26, 371–399.

Schmid, S.M., Bernoulli, D., Fügenschuh, B., Matenco, L., Schefer, S., Schuster, R., Tischler, M., Ustaszewski, K., 2008. The Alps-Carpathians-Dinarides-connection: a correlation of tectonic units. Swiss J. Geosci 101, 139–183.

Scholle, P.A., Arthur, M.A., 1980. Carbon-isotope fluctuations in Cretaceous pelagic limestones: potential stratigraphic and petroleum exploration tool. AAPG Bulletin 64, 67–87.

Sinton, C.W., Duncan, R.A., 1997. Potential links between ocean plateau volcanism and global ocean anoxia at the Cenomanian-Turonian boundary. Economic Geology, 92, 7–8.

Steuber, T., Löser, H., 2000. Species richness and abundance patterns of Tethyan Cretaceous rudist bivalves (Mollusca: Hippuritacea) in the central-eastern Mediterranean and Middle East, analysed from a palaeontological database. Palaeogeography, Palaeoclimatology, Palaeoecology 162, 75–104.

Steuber, T., Korbar, T., Jelaska, V., Gusic, I., 2005. Strontium isotope stratigraphy of Upper Cretaceous platform carbonates of the island of Brac (Adriatic Sea, Croatia): implications for global correlation of platform evolution and biostratigraphy. Cretaceous Research 26, 741–756.

Strauss, H., 2006. Anoxia through time. In: Neretin, L.N. (Ed.), Past and Present Water Column Anoxia. NATO Science Series. IV. Earth and Environmental Sciences. Springer, Netherlands, 3–19.

Sullivan, D.L., Brandon, A.D., Eldrett, J., Bergman, S.C., Wright, S., Minisini, D., 2020. High resolution osmium data record three distinct pulses of magmatic activity during cretaceous Oceanic Anoxic Event 2 (OAE-2). Geochimica et Cosmochimica Acta, 285, 257–273.

Swart, P.K., Oehlert, A.M., 2018. Revised Interpretations of Stable C and O Patterns in Carbonate Rocks Resulting from Meteoric Diagenesis, Sedimentary Geology 364, 14–23.

Tari, V., 2002. Evolution of the Northern and Western Dinarides: A Tectonostratigraphic Approach. European Geosciences Union: Stephan Mueller Special Publication Series, 1, 223–236.

Tišljar, J., Velić, I., Vlahović, I., 1994. Facies diversity of the Malmian platform carbonates in Western Croatia as a consequence of synsedimentary tectonics. Géologie Méditerranéenne XXI/3–4, 173–176.

Tišljar, J., Vlahović, I., Velić, I., Matičec, D., Robson, J., 1998. Carbonate facies evolution from the Late Albian to Middle Cenomanian in Southern Istria (Croatia): Influence of synsedimentary tectonics and extensive organic carbonate production. Facies 38, 137–152.

Tišljar, J., Vlahović, I., Velić, I., Sokač, B., 2002. Carbonate Platform megafacies of the Jurassic and Cretaceous deposits of the Karst Dinarides. Geologia Croatica 55/2, 139–170.

Tsikos, H., Jenkyns, H.C., Walsworth-Bell, B., Petrizzo, M.R., Forster, A., Kolonic, S., Erba, E., Premoli Silva, I., Bass, M., Wagner, T., Sinnghe Damsté, J.S., 2004. Carbon-isotope stratigraphy recorded by the Cenomanian–Turonian oceanic anoxic event: correlation and implications based on three key-localities. Journal of the Geological Society, London 161, 711–720.

Turgeon, S.C., Creaser, R.A., 2008. Cretaceous oceanic anoxic event 2 triggered by a massive magmatic episode. Nature 454, 323–326.

Velić, I., 2007. Stratigraphy and Paleobiogeography of Mesozoic Benthic Foraminifera of the Karst Dinarides (SE Europe). Geologia Croatica 60/1, 1–114.

Velić, I., Tišljar, J., Vlahović, I., Matičec, D., Korbar, T., Moro, A., Ćosović, V., 2002. Geological evolution of Istria (NW part of the Adriatic Carbonate Platform, Croatia). In: Vlahović, I, Korbar, T (ed.) 6th International Congress on Rudists, Rovinj. Abstracts and Excursion Guidebook, Zagreb, 83–93.

Velić, I., Tišljar, J., Vlahović, I., Matičec, D., Bergant, S., 2003. Evolution of the Istrian part of the Adriatic Carbonate Platform from the Middle Jurassic to the Santonian and Formation of the Flysch Basin During the Eocene: Main Events and Regional Comparison. Field Trip Guidebook. 22nd IAS Meeting of Sedimentology, Opatija, September 17–19, Zagreb, 3–18.

Vlahović, I., Tišljar, J., Velić, I., 1994. Influence of synsedimentary tectonics and eustatic changes on depositions of the Cenomanian platform carbonates in Istria (Western Croatia). Geologie Mediterraneenne 21 (3–4), 189–193.

Vlahović, I., Korbar, T., Moro, A., Velić, I., Skelton, P.W., Fuček, L., Tišljar, J., 2002a. Latest Cenomanian to earliest Turonian platform drowning and Turonian recovery of shallow-water platform deposition in southern Istria. Abstracts and Excursion Guidebook, Sixth International Congress on Rudists (Rovinj, Croatia), 152.

Vlahović, I., Tišljar, J., Fuček, L., Oštrić, N., Prtoljan, B., Velić, I., Matičec, D., 2002b. The origin and importance of the dolomite-limestone breccia between the Lower and Upper Cretaceous deposits of the Adriatic Carbonate Platform: An example from Ćićarija Mt. (Istria, Croatia), Geologia Croatica 55/1:45–55.

Vlahović, I., Tišljar, J., Velić, I., Matičec, D., Skelton, P.W., Korbar, T., Fuček, L., 2003. Main events recorded in the sedimentary succession of the Adriatic Carbonate Platform from the Oxfordian to the Upper Santonian in Istria (Croatia). Field Trip Guidebook. 22nd IAS Meeting of Sedimentology, Opatija, September 17.–19. 2003., 19–56.

967 Vlahović, I., Tišljar, J., Velić, I., Matičec, D., 2005. Evolution of the Adriatic Carbonate
968 Platform: Paleogeography, main events and depositional dynamics. Paleogeography
969 Paleoclimatology Paleoecology 220, 333–360.
970 Vlahović, I., Mikša, G., Mrinjek, E., Hasiotis, S.T., Velić, I., Tišljar, J., Matičec, D., 2011.
971 Response of tracemakers to temporary platform drowning: lower Cenomanian of
972 Southern Istria (Western Croatia). Palaios 26, 567–577.
973 Voigt, S., Gale, A.S., Voigt, T., 2006. Sea-level change, carbon cycling and palaeoclimate
974 during the Late Cenomanian of northwest Europe; an integrated palaeoenvironmental
975 analysis. Cretaceous Research, 27, 836–858.
976 Voigt, S., Erbacher, J., Mutterlose, J., Weiss, W., Westerhold, T., Wiese, F., Wilmsen, M.,
977 Wonik, T., 2008. The Cenomanian-Turonian of the Wunstorf section (North Germany):
978 global stratigraphic reference section and new orbital time scale for Oceanic Anoxic
979 Event 2. Newsletter on Stratigraphy 43/1, 65–89.
980 Wagreich, M., Bojar, A.V., Sachsenhofer, R.F., Neuhuber, S., Egger, H., 2008. Calcareous
981 nannoplankton, planktonic foraminifera, and carbonate carbon isotope stratigraphy of
982 the Cenomanian–Turonian boundary section in the Ultrahelvetic Zone (Eastern Alps,
983 Upper Austria). Cretaceous Research 29, 965–975.
984 Wendler, I., 2013. A critical evaluation of carbon isotope stratigraphy and biostratigraphic
985 implications for Late Cretaceous global correlation, Earth Science Reviews, 126, 116-
986 146.
987 Wohlwend, S., Hart, M., Weissert, H., 2015. Ocean current intensification during the
988 Cretaceous oceanic anoxic event 2 – evidence from the northern Tethys. Terra Nova,
989 27, 147–155.
990

991 Fig. 1: Study area. a) Global position of the study area in Croatia; b) Regional setting including
992 location of previous OAE2-related research areas; c) Local position of the Barban section; d)
993 Local position of the Premuda section; e) Orthophoto (with Digital Relief Model - DRM) of the
994 Barban section exposure (A – starting point, D – end point); f) Orthophoto (with DRM) of the
995 Premuda section exposure (A – starting point, B – end point).
996
997 Fig. 2: Paleogeographic setting of the study area. a) The wider Perimediterranean region (prior
998 to approximately 100 Mya) with paleogeographically reconstructed locations of the Barban
999 (BS) and Premuda (PS) sections within the Adriatic Carbonate Platform (AdCP) (modified after
1000 Blakey 2010, and references therein); b) Peninsula Istria during the late Cenomanian to early
1001 Turonian (Brčić et al. 2017) with location of the Barban section; c) Premuda island during the
1002 late Cenomanian to Santonian with location of the study section.
1003
1004 Fig. 3: Detailed measured stratigraphic sections at the Barban and Premuda sites, indicating
1005 rock formations names (lithostratigraphy), age, and lithologies and fossils present.
1006
1007 Fig. 4: Detailed stratigraphic sections measured at Barban and Premuda with photomicrographs
1008 of the typical facies present (SMF – shallow-marine facies, TF – transition shallow-marine to
1009 deeper-marine facies, DMF – deeper-marine facies; see Section 5), correlated (grey interval)
1010 on the basis of their carbon isotope compositions. Isotope curves were constructed by
1011 connecting all individual data points. Photomicrograph scale = 1 mm.
1012
1013 Fig. 5: Correlation of the Barban and Premuda sections with the reference Eastbourne section
1014 (Pearce et al. 2009) using stable-isotope data and benthic/planktonic foraminifera biozones.

Green dotted line represents CT boundary. TOC and insoluble residue data for the Barban section are also shown.

Fig. 6: Block diagrams of paleoenvironmental conditions from late Cenomanian to early Coniacian in the wider research area: NWI – North-western Istria; BS – paleogeographic location of the Barban section; PS – paleogeographic location of the Premuda section (see text for details).

Fig. 7: Field photographs of the Barban section: **a)** Thin-bedded upper Cenomanian deposits at the western part of the Barban section (see Fig. 1e); **b)** Thin-layered transition between the Milna (shallow-marine) and Sv. Duh (with pelagic influence) Formations (oscillating transgression, see Section *5.2.*; hammer for scale is 32 cm long); **c)** Radiolitid rudist biostrome of the Milna Formation (upper Cenomanian); **d)** Transition shallow-marine to deeper-marine facies with a stylolite (black dotted line) between the Sv. Duh (SD, calcisphere wackestone) and Gornji Humac Formations (GH, peloidal grainstone).

Fig. 8: Field photographs of the Premuda section: **a)** Radiolitid (Ra) and chondrodontid (Ch) lithostrome floatstone of the Milna Formation; **b)** Coarse lithoclasts (lth) and other shallow-marine material re-deposited in bioclastic-lithoclastic lithosome intercalated within the calcisphere wackestones in the lower part of the Veli Rat Formation; **c)** and **d)** Lithoclasts (lth) of the shallow-marine Milna Formation deposits within the deeper-marine Veli Rat Formation deposits; **e)** subvertical layers (interval between 44 and 60 m) of the Premuda section (view to the east; see Figs. 1 and 3).

Fig. 9: Photomicrographs of benthic foraminifera from the Barban and Premuda sections (scale = 0.5 mm): **a)** and **b)** *Pastrickella balcanica* (Cherchi, Radoičić and Schroeder), samples Plo-26b and BB-6; **c)** and **d)** *Heteroporella lepina* Praturlon, sample BB-32; **e)** *Heteroporella lepina* Praturlon, sample BB-32; **f)** *Thaumatoporella parvovesiculifera* (Raineri), sample Plo-37a; **g)** and **h)** *Cisalveolina* sp., samples Plo-16b and Plo-24 ; **i)** *Peneroplis planatus* (Fichtel and Moll), sample Plo-34; **j)** *Scandonea* sp., sample BB-11; **k)**, **l)** and **m)** *Cuneolina* cf. *pavonia* (d'Orbigny), samples BB-06 and BB-04; **n)** *Vidalina radoicicae* Cherchi and Schroeder, sample BB-11; **o)** *Pseudonummoloculina heimi* (Bonet), sample BB-06; **p)**, **q)** and **r)** *Chrysalidina gradata* d'Orbigny, samples BB-06 and Plo-03; **s)** *Pseudorhapydionina dubia* De Castro, sample BB-06; **t)** *Idalina* cf. *antiqua* (Munier-Chalmas et Schlumberger), sample BB-06; **u)** *Nezzazata* cf. *gyra* (Smout), sample BB-06; **v)** *Nezzazata simplex* Omara, sample BB-04.

Fig. 10: Photomicrographs of planktonic foraminifera from the Barban and Premuda sections (scale = 200 μm): **a)** *Marginotruncana* cf. *renzi* (Gandolfi), sample Plo-72; **b)** *Heterohelix* sp., sample Plo-71; **c)** *Marginotruncana sigali* (Reichel), sample Plo-70; **d)** *Dicarinella* sp., sample Plo-70; **e)** *Marginotruncana schneegansi* (Sigal), sample Plo-70; **f)** *Archaeoglobigerina* cf. *blowi* Pessagno, sample Plo-65; **g)** *Praeglobotruncana gibba* (Klaus), sample Plo-61; **h)** *Helvetoglobotruncana* cf. *helvetica* (Bolli), sample Plo-59; **i)** *Helvetoglobotruncana praehelvetica* (Trujillo), sample Plo-53; **j)** *Whiteinella* cf. *paradubia* (Sigal), sample Plo-52a; **k)** *Helvetoglobotruncana praehelvetica* (Trujillo), sample Plo-52a; **l)** *Dicarinella imbricata* (Monrod), sample Plo-51; **m)** *Whiteinella* cf. *archaeocretacea* Pessagno, sample Plo-42b; **n)** *Helvetoglobotruncana praehelvetica* (Trujillo), sample Plo-37b; **o)** *Whiteinella* cf. *paradubia* (Sigal), sample Plo-22.

Table 1: Results (values) of stable isotope analysis of 122 samples (81 from Barban and 41 from Premuda section) and TOC and Insoluble Residue Analyses (81 samples from Barban section). - *Appendix/supplement*

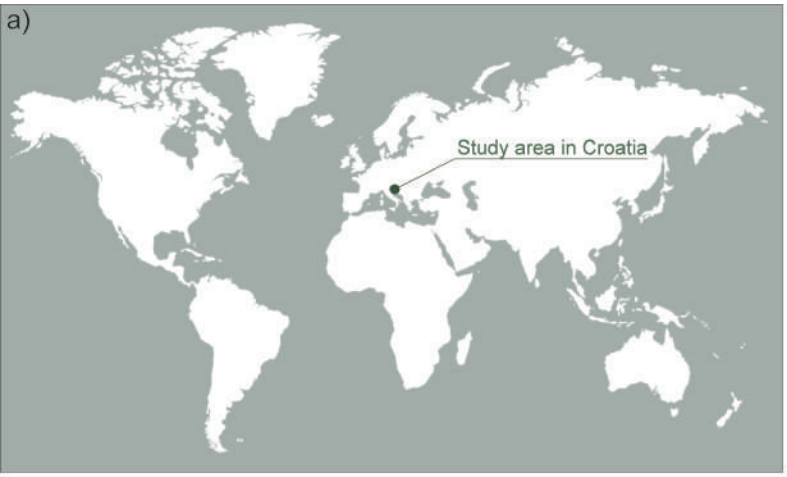
a)
Study area in Croatia


c)
Slovenia
Croatia
Buzet
Opatija
Rijeka
Pazin
Poreč
Istria
Rovinj
Barban section
e
Adriatic sea
Kvarner
Pula
Cres
Medulin
20 km


d)
Adriatic sea
Premuda island
Premuda section
f
Adriatic sea
2 km

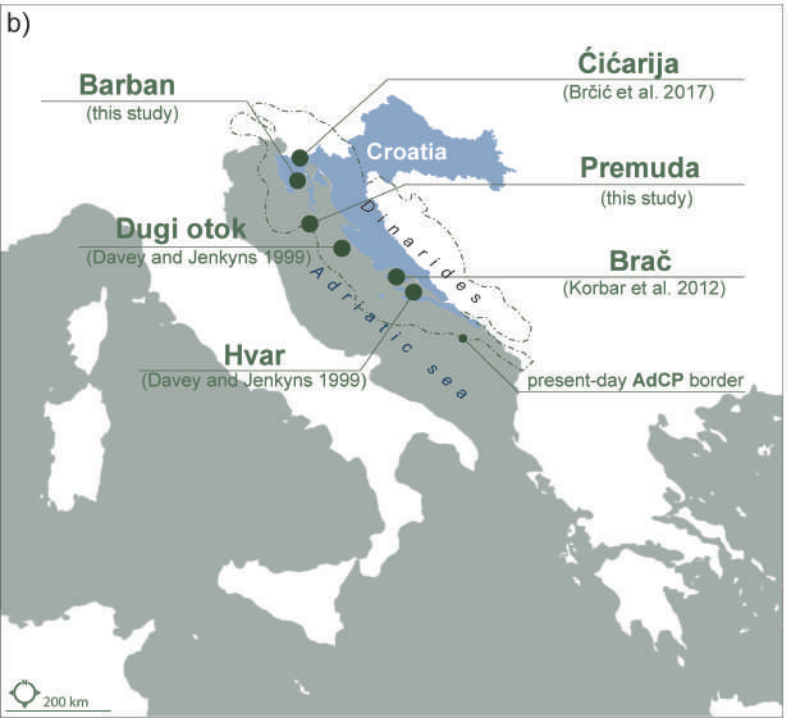
b)
Barban
(this study)
Ćićarija
(Brčić et al. 2017)
Croatia
Premuda
(this study)
Dugi otok
(Davey and Jenkyns 1999)
Dinarides
Brač
(Korbar et al. 2012)
Adriatic sea
Hvar
(Davey and Jenkyns 1999)
present-day AdCP border
200 km

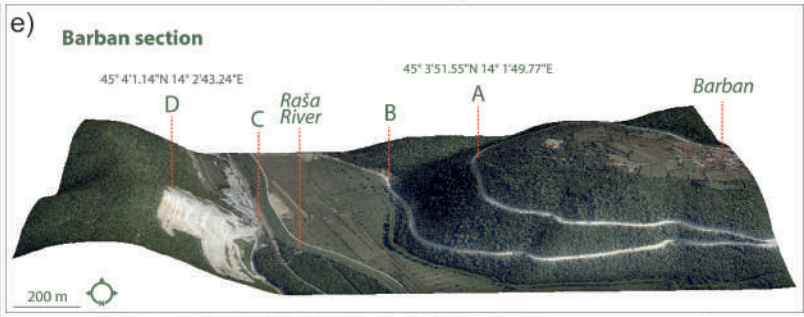
e)
Barban section
45° 4'1.14"N 14° 2'43.24"E
45° 3'51.55"N 14° 1'49.77"E
D
C
Raša
River
B
A
Barban
200 m


f)
Premuda section
A 44°18'9.32"N 14°40'9.48"E
B 44°18'6.39"N 14°40'6.86"E
50 m


a)
Eurasia
Iberia
Balkans-Rhodope
Atlantic
Deep marine
Alpine Tethys
Neotethys
BS
PS
AdCP
Shallow marine
Apulia
Exposed land
Neotethys
North Africa
500 km

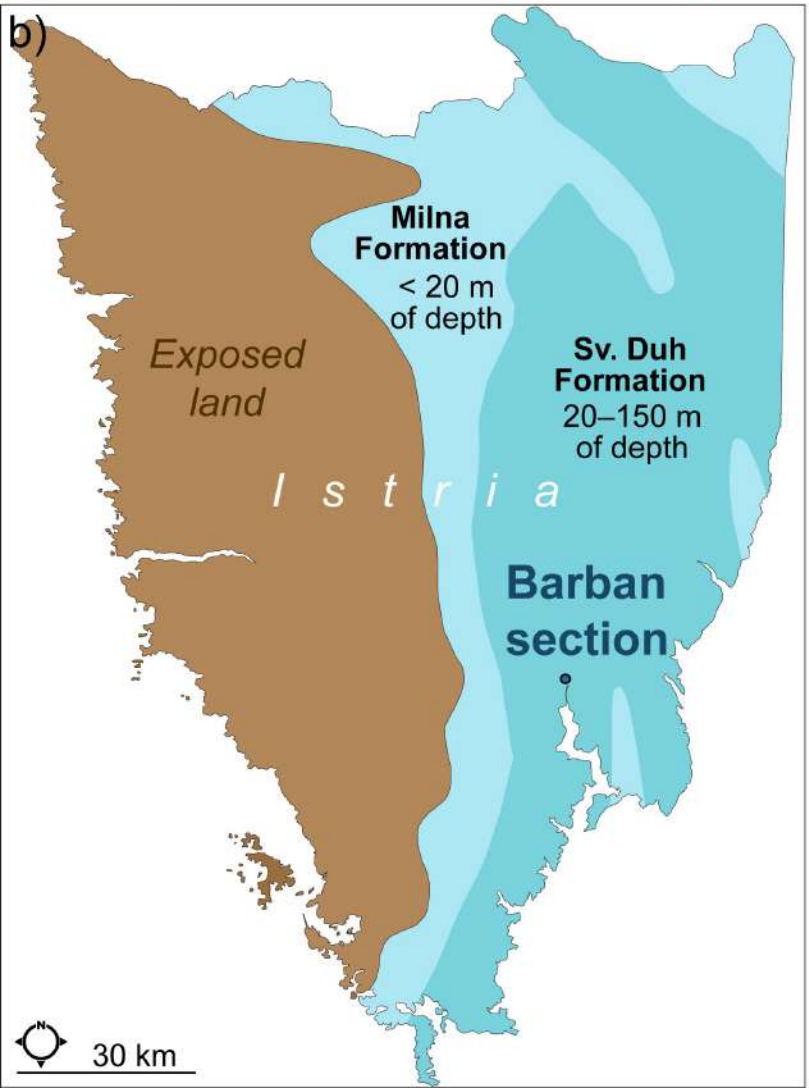
b)
Milna Formation
< 20 m of depth
Exposed land
Sv. Duh Formation
20–150 m of depth
Istria
Barban section
30 km

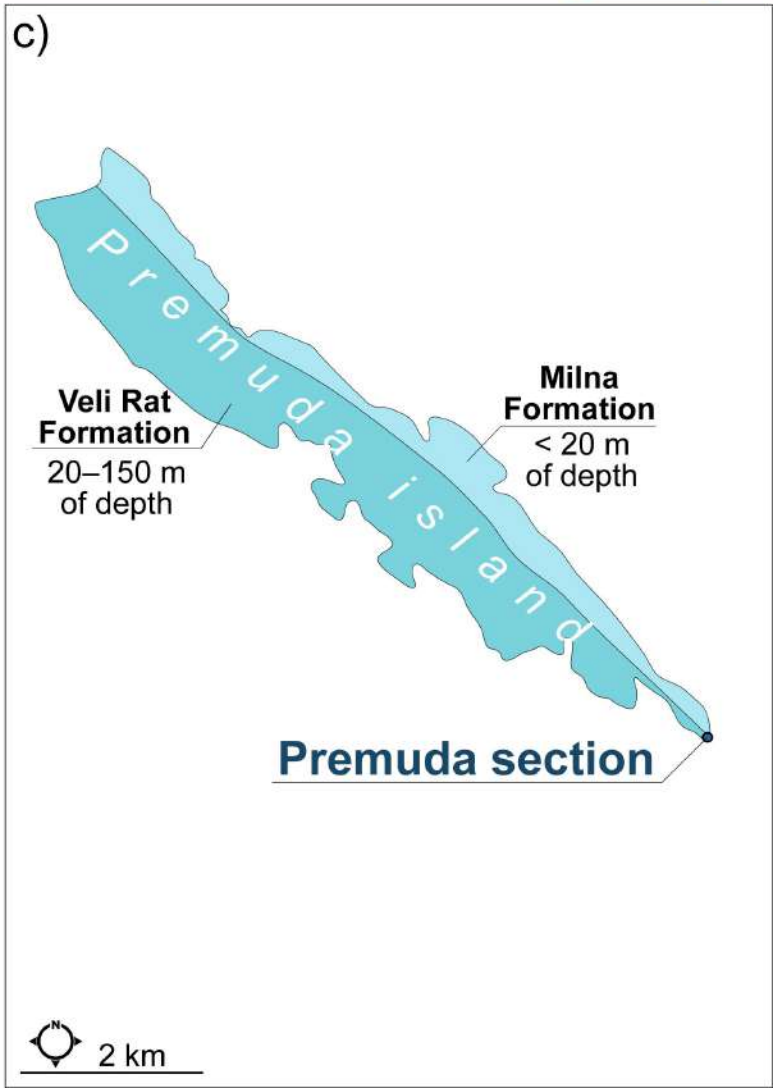
c)
Premuda island
Veli Rat Formation
20–150 m of depth
Milna Formation
< 20 m of depth
Premuda section
2 km

Barban section

Lithostrat. | Scale (m) | Age | Lithology | Description | Algae / Rudist / Benthic Foraminifera / Planktonic Foraminifera

Milna Formation | Sv. Duh Formation | Gornji Humac F.

Cenomanian | Turonian

Shallowing-upward interval

Deepening-upward interval

Bioclastic--skeletal F (rudist lithostrome)

Small-scale clinoforms with peloidal--ooid P-G with normal grading toward calcisphere W

Calcisphere W enriched with fine-grained bioclastic detritus

Calcisphere M-W

Calcisphere W enriched with fine grained bioclastic detritus

Calcisphere M-W

Calcisphere W enriched with fine-grained bioclastic detritus

Calcisphere M-W

Calcisphere W enriched with fine-grained bioclastic detritus

Peloidal--skeletal--bioclastic P intercalated with microbial laminites and rare bioclastic--skeletal F

Heteroporella lepina

Distefanella sp.

Praeglobotruncana sp.

Rotalipora sp.

Broeckina (Pastrikella) balcanica

Vidalina radoicicae

Chrysalidina gradata

Premuda section

Lithostrat. | Scale (m) | Age | Lithology | Description | Algae / Benthic Foraminifera / Planktonic Foraminifera

Milna F. | Veli Rat Formation

Cenomanian | Turonian | Con.

Slope deposits interval

Calcisphere M-W

Reworked slope fine-grained bioclastic detritus in deeper-marine calcisphere W

Calcisphere M-W

Calcisphere W enriched with fine-grained bioclastic detritus

Reworked coarse-grained bioclastic F intercalated with deeper-marine calcisphere W

Lithoclasts

Peloidal--skeletal--bio/lithoclastic P intercalated with microbial laminites and rare bioclastic--skeletal F

Heteroporella lepina

Vidalina radoicicae

Pseudorhapydionina dubia

Cisalveolina sp.

Chrysalidina gradata

Broeckina (Pastrikella) balcanica

Marginotruncana sigali

Dicarinella cf. *algeriana*

Dicarinella sp.

Dicarinella imbricata

Praeglobotruncana gibba

Dicarinella primitiva

Whiteinella archaeocretacea

Whiteinella praehelvetica

Praeglobotruncana sp.

Whiteinella cf. *paradubia*

Helvetoglobotruncana cf. *helvetica*

Archaeoglobigerina cf. *cretacea*

Archaeoglobigerina cf. *blowi*

Archaeoglobigerina sp.

- planktonic foraminifera
- ostracodes
- pithonellas
- echinoderm spines
- sponge spicules
- cb lamination
- shells
- benthic foraminifera
- rudist and rudist bioclast
- rudist lithostrome (*Radiolitidae congr.*)
- miliolidae
- *Decastronema* sp.
- algae (*Thaumatoporella* sp.)
- green algae (*Heteroporella lepina*)
- biodetritus
- bioturbations

M–mudstone W–wackestone P–packstone G–grainstone F–floatstone

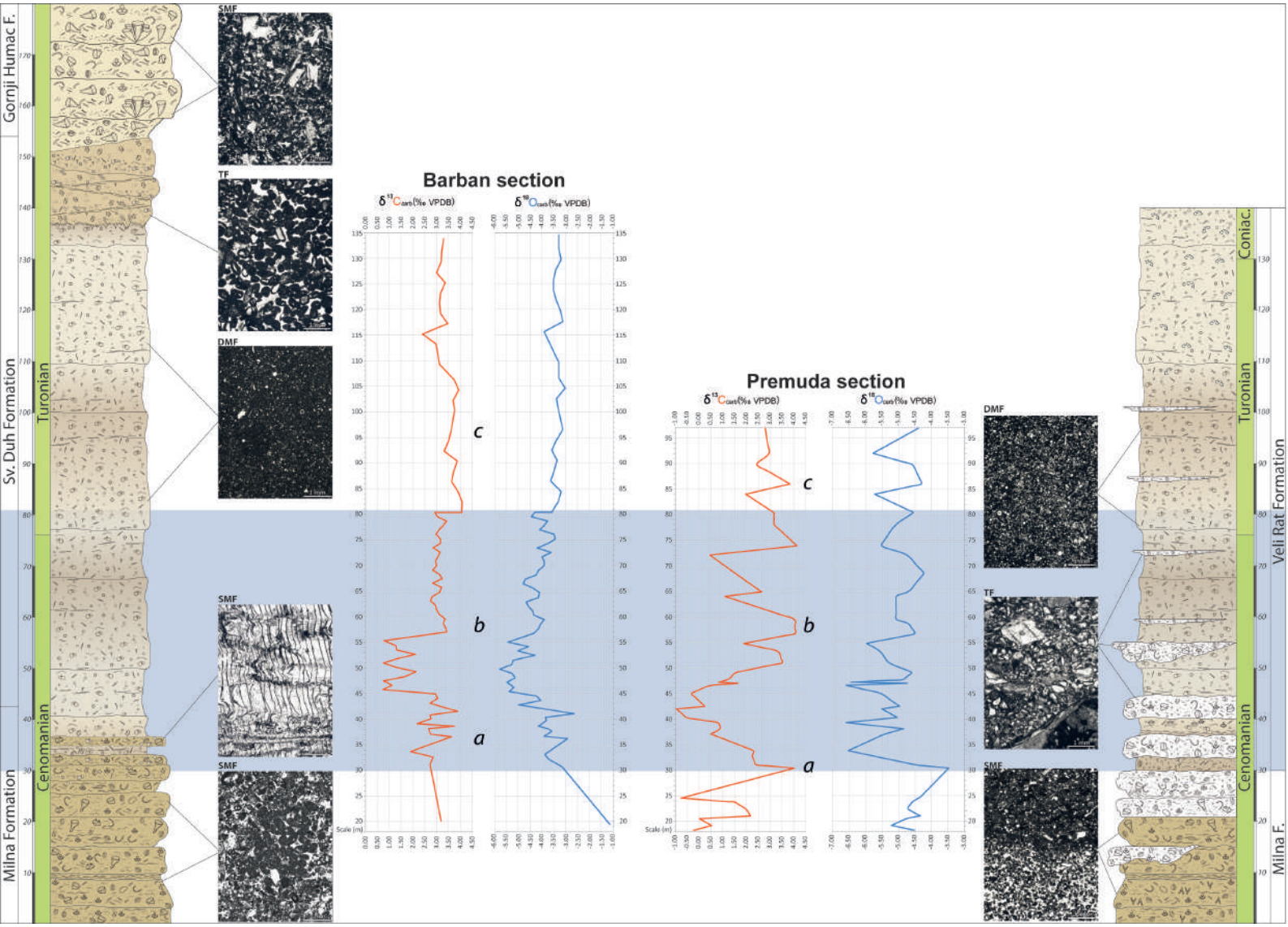
Gornji Humac F.
Sv. Duh Formation
Milna Formation
Turonian
Cenomanian
Coniac.
Veli Rat Formation
SMF
TF
DMF
Barban section
Premuda section
a
b
c

Stage
Benthic Foraminifers Biozones
Velić 2007 (AdCP, Dinaric karst)
Benthic Foraminifers Biozones
Chiocchini et al. 2008 (ACP, Lazio-Abruzzo)
Planktonic Foraminifers Biozones
Turonian
Cenomanian
Chrysalidina gradata
B. balcanica & C. conica
Vidalina radoicicae & Chrysalidina gradata
Chrysalidina gradata & Pseudocyclammina sphaeroidea
P. sphaeroidea & S. samnitica
Pseudorhapydionina dubia & Pseudorhapydionina laurinensis
Chrysalidina gradata & P. reicheli
Nezzazatinella cf. aegyptiaca & Nummoloculina cf. irregularis
R. cushmani
Whiteinella archaeocretacea
Helvetoglobotruncana helvetica
Barban section
Premuda section
Eastbourne r. c.
Insoluble Residue (%)
TOC (% x 100)
δ13Ccarb (‰VPDB)
δ18Ocarb (‰VPDB)
Scale (m)
a
b
c

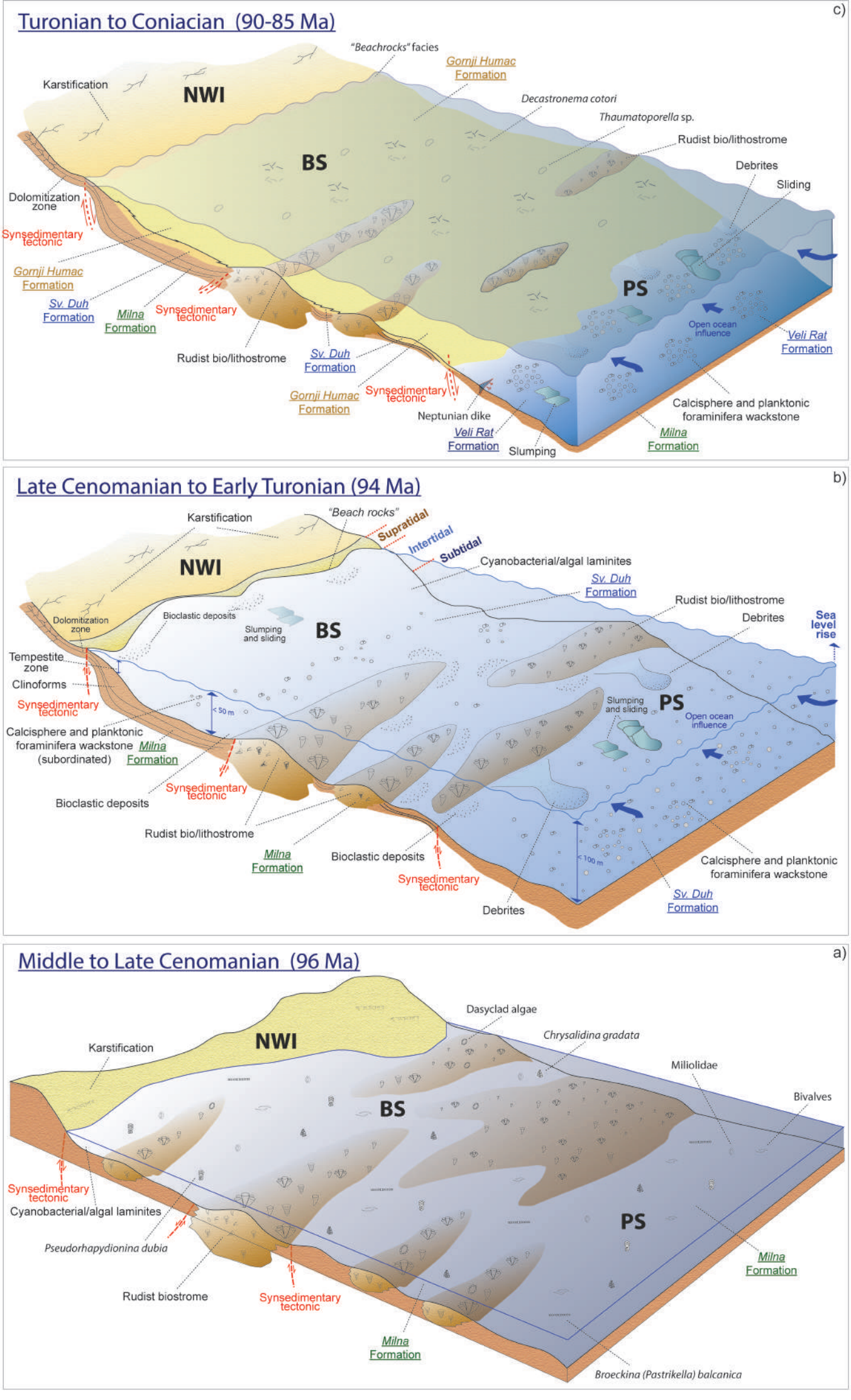
c)
Turonian to Coniacian (90-85 Ma)
"Beachrocks" facies
Gornji Humac Formation
Karstification
NWI
Decastronema cotori
Thaumatoporella sp.
Rudist bio/lithostrome
BS
Debrites
Sliding
Dolomitization zone
Synsedimentary tectonic
Gornji Humac Formation
Sv. Duh Formation
Milna Formation
Synsedimentary tectonic
PS
Open ocean influence
Veli Rat Formation
Rudist bio/lithostrome
Sv. Duh Formation
Gornji Humac Formation
Synsedimentary tectonic
Calcisphere and planktonic foraminifera wackstone
Neptunian dike
Veli Rat Formation
Slumping
Milna Formation
b)
Late Cenomanian to Early Turonian (94 Ma)
Karstification
"Beach rocks"
Supratidal
Intertidal
Subtidal
NWI
Cyanobacterial/algal laminites
Sv. Duh Formation
Rudist bio/lithostrome
Debrites
Sea level rise
Dolomitization zone
Bioclastic deposits
Slumping and sliding
BS
Tempestite zone
Clinoforms
Synsedimentary tectonic
< 50 m
Slumping and sliding
PS
Open ocean influence
Calcisphere and planktonic foraminifera wackstone (subordinated)
Milna Formation
Synsedimentary tectonic
Bioclastic deposits
Rudist bio/lithostrome
Milna Formation
Bioclastic deposits
Synsedimentary tectonic
< 100 m
Calcisphere and planktonic foraminifera wackstone
Debrites
Sv. Duh Formation
a)
Middle to Late Cenomanian (96 Ma)
Dasyclad algae
Chrysalidina gradata
Karstification
NWI
Miliolidae
Bivalves
BS
Synsedimentary tectonic
Cyanobacterial/algal laminites
Pseudorhapydionina dubia
PS
Milna Formation
Rudist biostrome
Synsedimentary tectonic
Milna Formation
Broeckina (Pastrikella) balcanica

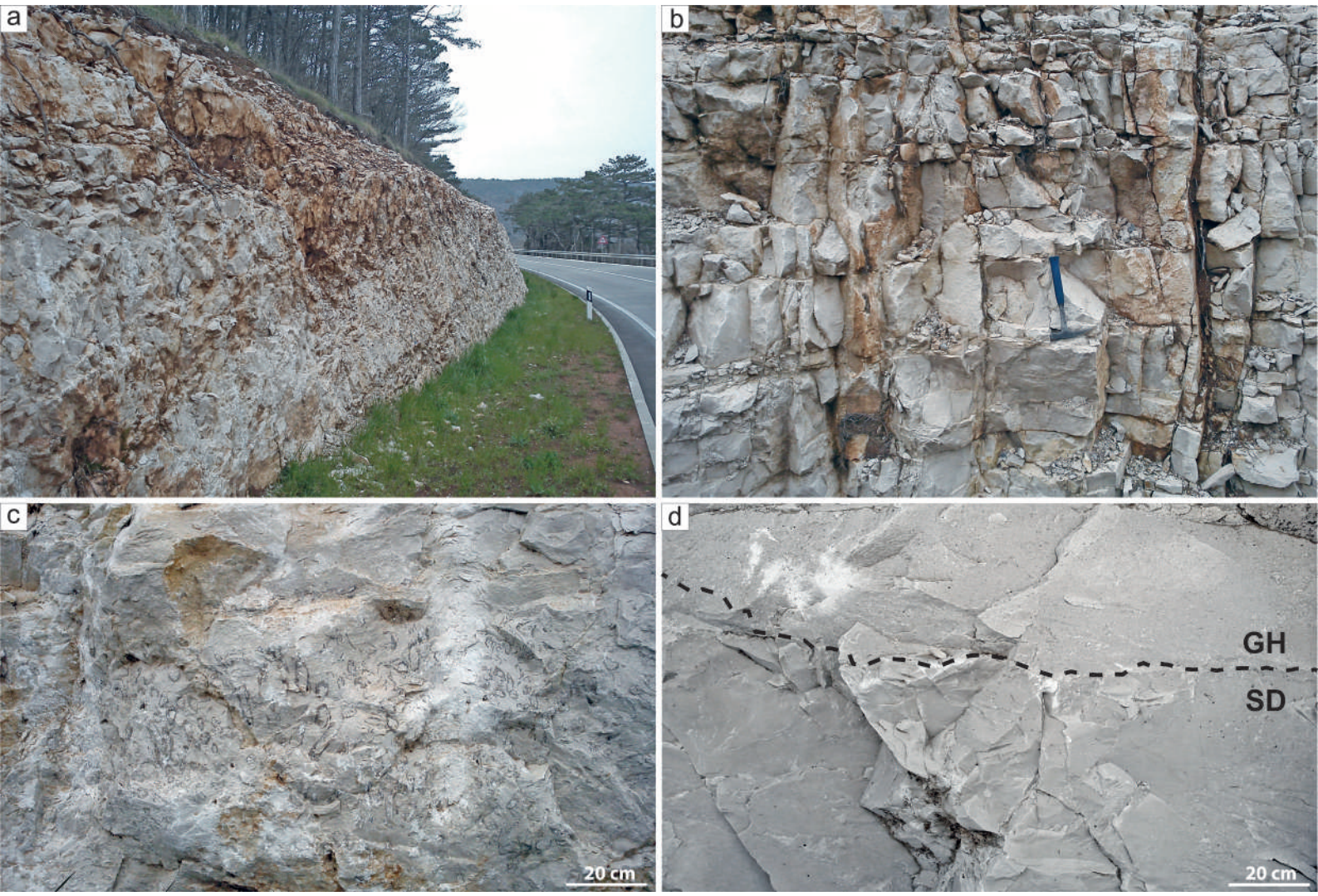
a
b
c
d
20 cm
GH
SD
20 cm

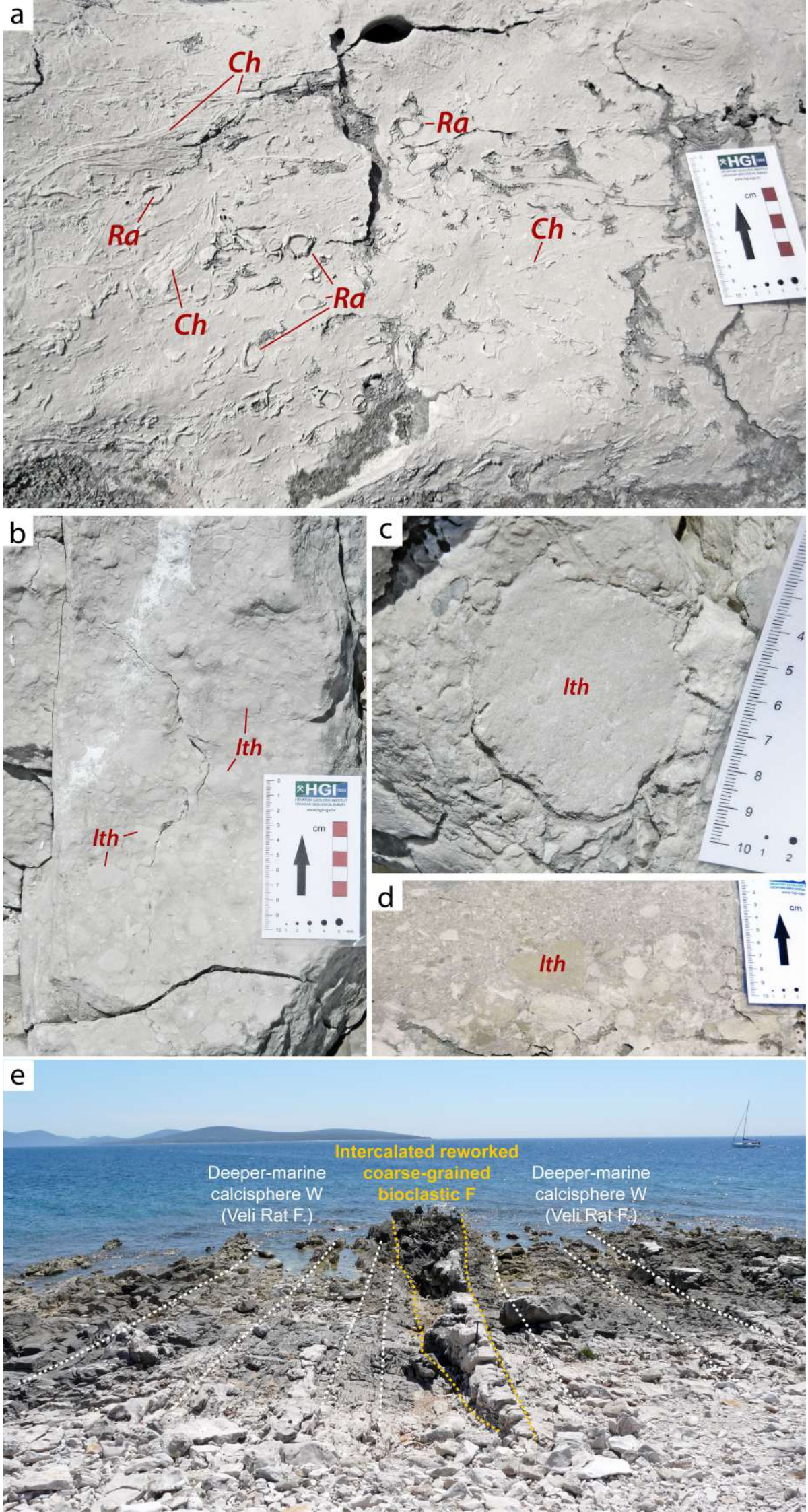
a
Ch
Ra
Ra
Ch
Ra
Ch
b
lth
lth
c
lth
d
lth
e
Deeper-marine calcisphere W (Veli Rat F.)
Intercalated reworked coarse-grained bioclastic F
Deeper-marine calcisphere W (Veli Rat F.)

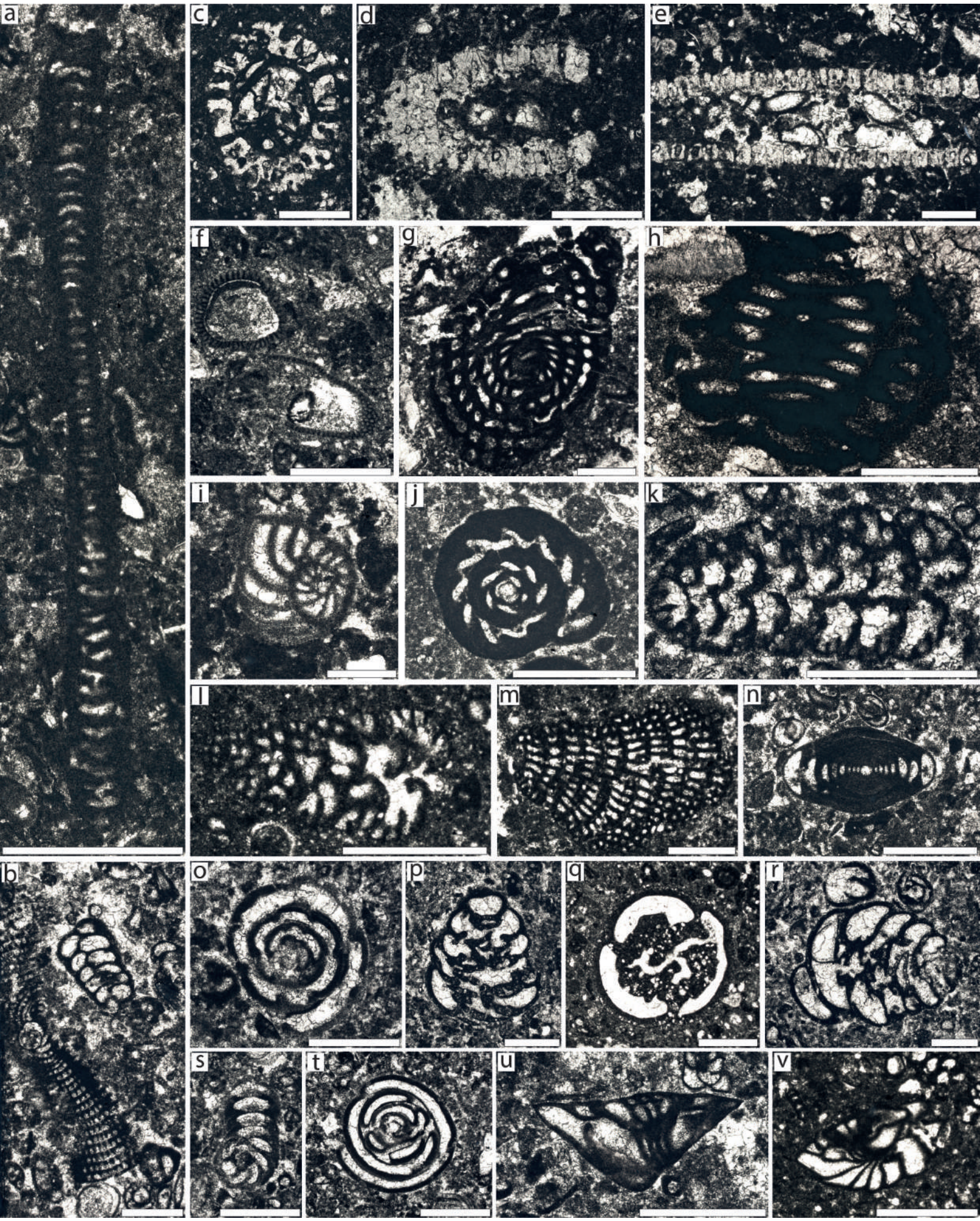
a
c
d
e
f
g
h
i
j
k
l
m
n
b
o
p
q
r
s
t
u
v

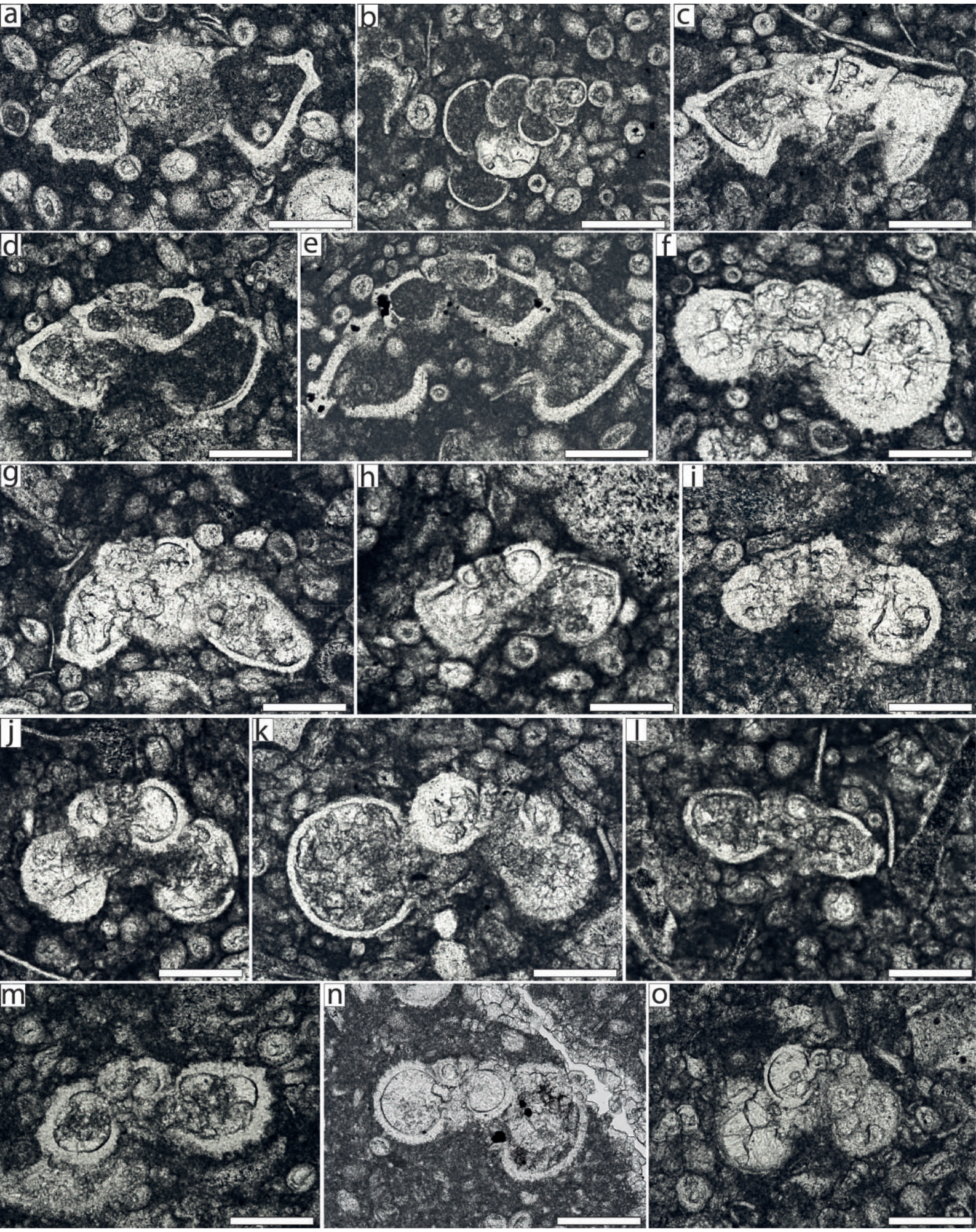
a
b
c
d
e
f
g
h
i
j
k
l
m
n
o